Electronic Supplementary Material (ESI) for ChemComm.

Supporting Information

Ionic Liquid-functionalized amphiphilic Janus material as Pickering interfacial catalyst for asymmetric sulfoxidation in water

CONTENT:

1. Synthetic details of **HO-SiO_2-*IL*-Ti(salen)$_x$ (x= 0.05, 0.07, 0.09, 0.11), HO-SiO_2-Ti(salen),** and **SiO_2-*IL*-Ti(salen)**.

1.1 Materials and reagents

Tetraethylorthosilicate (TEOS) was obtained from Aldrich. *N*-[3-(triethoxysilyl)propyl]- 4,5-dihydroimidazole and 3-aminopropyltriethoxysilane (APTES) were obtained from Aladdin. Phenyl methyl sulfide, phenyl ethyl sulfide, 4-methoxyphenyl methyl sulfide, 2-methoxyphenyl methyl sulfide, and 4-bromophenyl methyl sulfide were obtained from J&K. 2-*tert*-Butyl phenol was purchased from Alfa Aesar. Other commercially available chemicals were obtained from local suppliers. All solvents were purified by standard procedures. Silica nanoparticles were synthesized according to the typical Stöber method.[1] Ethyl phenyl sulfide, *n*-butyl phenyl sulfide, and *n*-hexyl phenyl sulfide were synthesized according to Ref.[2] [(R,R')-[*N,N'*-(3,5-di-tert-butylsalicylidene)- 1,2-cyclohexanediaminato] titanium(IV) di-isopropyl (denoted as neat complex) was synthesized according to the described procedure in Ref.[3] (R,R)-[N-(3,5-di-tert-butylsalicylidene)-N′-(3-tert-butyl-5-chloro-methylsalicylidene)-1,2-cyclohexanediaminato] titanium(IV) di-isopropyl (denoted as asymmetric chiral salen Ti^{IV} complex) was synthesized as described procedure in Ref.[4]

1.2 Methods

FT-IR spectrum were obtained using potassium bromide pellets with a resolution of 4 cm^{-1} and 32 scans in the range of 400–4000 cm^{-1} using an AVATAR 370 Thermo Nicolet spectrophotometer. NMR spectrum of samples was recorded on a BRUKER AVANCE-500 spectrometer with TMS as an internal standard. TEM images were obtained on a Microscope Tecnai F20 at an accelerating voltage of 200 kV. Dynamic light scattering (DLS) was performed

using a ZS90 Laser Particle Size Analyzer (Malvern UK). Samples were dispersed in ethanol (20 mg. mL^{-1}) under ultrasonication for 30 min, giving rise to a uniform solution for DLS determination. Surface wettability of the samples was investigated by the analysis of the water contact angles (WCA) on TX500TM (Kono Corp.) Samples were directly compressed without the aid of binder. A drop of deionized water was then placed on it and imaged by camera. Microscope images of sulfide-in-water emulsions were obtained on BX53M (Olympus Corp.). Titanium contents in the samples were determined by inductively coupled plasma mass spectrometry (ICP-MS) on a NexION 300X analyzer (Perkin-Elmer Corp.). The conversion and chemoselectivity to chiral sulfoxides were analyzed by a 6890 N gas chromatograph (Agilent Co.) equipped with a capillary column (HP19091G-B213, 30 m × 0.32 mm × 0.25 lm) and a FID detector. Enantioselectivity (Ee value) of chiral sulfoxides was determined by HPLC analysis using Daicel Chiralpak AD column.

1.3 Synthesis of alkoxysilane reagents of $(C_2H_5O)_3$Si-*IL*/Ti(salen) and $(C_2H_5O)_3$Si-Ti(salen)

$(C_2H_5O)_3$Si-*IL*/Ti(salen) was synthesized through *N*-alkylation of terminal imidazole groups in *N*-[3-(triethoxysilyl)propyl]-4,5-dihydroimidazole with methyl chloride group ($–CH_2Cl$) at 5-position of asymmetric chiral salen Ti^{IV} complex, as shown in Scheme 1. Asymmetric chiral salen Ti^{IV} complex (5 mmol, 3.51 g) was mixed with *N*-[3-(triethoxysilyl)propyl]-4,5- dihydroimidazole (5.2 mmol, 1.43 g) in dry toluene (100 mL). The corresponding mixture was stirred at 110 ^oC for 24 h under argon atmosphere. After removal of solvent, the residue was wash was *n*-hexane, and then dried under vacuum at room temperature for 12 h, giving $(C_2H_5O)_3$Si-*IL*/Ti(salen). FT-IR (KBr): γ_{max}/cm^{-1} 3400, 2953, 2864, 1645, 1564, 1480, 1438, 1390, 1349, 1326, 1243, 1219, 1157, 1120, 1099, 805, 764, 742, 713, 621, 509, 470. ^1H NMR (500 MHz, $CDCl_3$): δ (ppm): 7.63-6.96

(m, 4 H, Ar*H*), 4.63 (m, 1 H, N-C*H*-N in IL), 4.36 (m, 2 H, C*H*=N), 3.80-3.79 (m, 6 H, CH_3-CH_2-O), 3.70-3.68 (m, 2 H, CH_3-C*H*-CH_3 of ^{i}PrO), 3.49 (m, 2 H, -N-CH_2-Ph-), 3.28 (m, 2 H, N-C*H*-C*H*-N in cyclohexyl), 2.95-2.94 (m, 6 H, CH_2-CH_2-N-CH_2-CH_2-N in IL), 1.52 (m, 2 H, Si-CH_2-CH_2-CH_2-N), 1.66 (m, 2 H, Si-CH_2-CH_2-CH_2-N), 1.41-1.39 (m, 8 H, CH-CH_2-CH_2-CH_2-CH_2-CH in cyclohexyl), 1.31-1.29 (m, 27 H, H in *t*-butyl), 1.21 (m, 21 H, CH_3-CH_2-O-Si and CH_3-CH-CH_3 of ^{i}PrO), 0.56 (m, 2 H, Si-CH_2-CH_2-CH_2-N).

As shown in Scheme 1, the preparation procedure of $(C_2H_5O)_3$Si-Ti(salen) was similar to that of $(C_2H_5O)_3$Si-*IL*/Ti(salen), except for the use of 3-aminopropyltriethoxysilane instead of *N*-[3-(triethoxysilyl)propyl]-4,5-dihydroimidazole during *N*-alkylation. FT-IR (KBr): γ_{max}/cm^{-1} 3432, 2960, 2930, 2864, 1747, 1645, 1552, 1538, 1516, 1472, 1387, 1266, 1100, 884, 808, 805, 672, 586, 469. ^{1}H NMR (500 MHz, $CDCl_3$): δ (ppm): 7.36-6.97 (m, 4 H, Ar*H*), 4.41-4.33 (m, 2 H, C*H*=N), 3.74-3.69 (m, 6 H, CH_3-CH_2-O), 3.58-3.57 (m, 2 H, CH_3-C*H*-CH_3 of ^{i}PrO), 3.48 (m, 2 H, -N-CH_2-Ph-), 3.30-3.28 (m, 2 H, N-C*H*-C*H*-N in cyclohexyl), 1.59 (m, 2 H, Si-CH_2-CH_2-CH_2-N), 1.54 (m, 2 H, Si-CH_2-CH_2-CH_2-N), 1.43-1.40 (m, 8 H, CH-CH_2-CH_2-CH_2-CH_2-CH in cyclohexyl), 1.38-1.34 (m, 27 H, H in *t*-butyl), 1.24-1.23 (m, 21 H, CH_3-CH_2-O-Si and CH_3-CH-CH_3 of ^{i}PrO), 0.67 (m, 2 H, Si-CH_2-CH_2-CH_2-N).

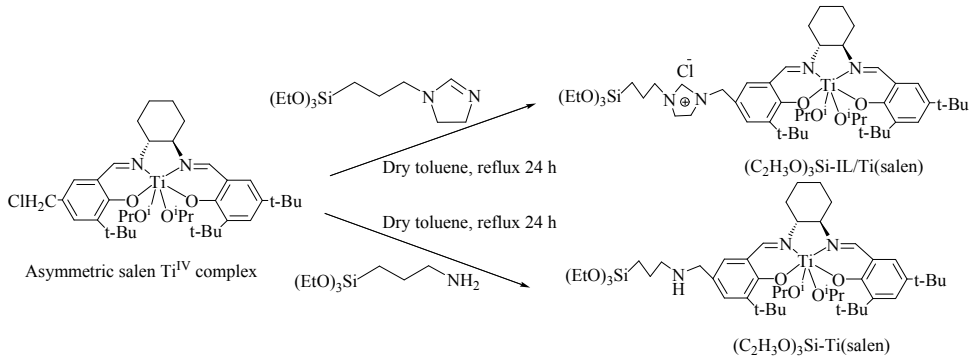

Scheme S1 Synthesis of alkoxysilane reagents of $(C_2H_5O)_3$Si-*IL*/Ti(salen) and $(C_2H_5O)_3$Si-Ti(salen).

1.4 Preparation of *IL*-functionalized JNPs catalyst of **HO-SiO$_2$-*IL*-Ti(salen)$_x$** (where x represented the titanium content in samples, x= 0.05, 0.07, 0.09, and 0.11 mmol/g)

Janus-type catalysts of **HO-SiO$_2$-*IL*-Ti(salen)$_x$** were synthesized through a classic method based on the Pickering emulsions of wax-in-water, as shown in Scheme S2.

Scheme S2 Schematic representation of **HO-SiO$_2$-*IL*-Ti(salen)$_x$** by wax emulsion method.

Synthesis of SiO_2 nanoparticles (denoted as SiO_2-OH). Silica nanoparticles which were synthesized according to the modified Stöber method[1] were treated with piranha solution (3:1 mixture of concentrated H_2SO_4 and 30% H_2O_2) at 80 °C and 350 rpm for 0.5 h. The treated silica nanoparticles were centrifuged (5000 rpm, 10 min), washed with deionized water, and dried at 80 °C under vacuum. FT-IR: γ_{max}/cm^{-1} 3437, 1630, 1080, 970, 798.

Synthesis of solid wax droplets trapped silica nanoparticles (denoted as wax@SiO_2-OH). Wax@SiO$_2$-OH were synthesized on the basis of a wax-in-water emulsion using cetyltrimethylammonium bromide (CTAB) as a surfactant.[5] SiO$_2$-OH (0.25 g) and paraffin wax (2.5 g) were added to the aqueous solution (20 mL) of CTAB with different concentration (0.36, 0.54, 0.72 mmol.L^{-1} and 0.90 mmol.L^{-1}). The SiO$_2$-OH particles became more hydrophobic with the surfactant concentration increasing, penetrating more deeply into the wax phase. It thus reduced the exposed surface of SiO$_2$-OH for modification.[6] The resulting mixtures were incubated at 75 °C for 0.5 h, and then vigorously stirred under 12 000 rpm for 10 min. After being rapidly cooled to room temperature, wax@SiO$_2$-OH droplets with various area of exposed SiO$_2$ surface

were obtained. The wax droplets were filtered, washed with deionized water to remove the excess and weakly attached silica nanoparticles, and then dried at 25 °C under vacuum for 24 h.

Synthesis of **HO-SiO_2-*IL*-Ti(salen)$_x$**. The obtained dried wax@SiO_2-OH (2.0 g) were mixed with $(C_2H_5O)_3$Si-*IL*/Ti(salen) (0.2 mmol, 0.2 g) in anhydrous methanol solution (20 mL). The mixtures were stirred at 25 °C under 100 rpm for 12 h. Exposed surface of SiO_2-OH in wax@SiO_2-OH was thus decorated with the *IL*/Ti(salen)-containing alkoxysilane reagent through silylation reaction, giving solid wax trapped wax@SiO_2-*IL*/Ti(salen). Then, chloroform was used to dissolve the paraffin wax at 40 °C, thereby releasing the *IL*/Ti(salen)-modified silica nanoparticles. After centrifugation, the residue was washed with chloroform and anhydrous ethanol for several times, and dried under vacuum at 40 °C for 24 h. The obtained samples were denoted as **HO-SiO_2-*IL*-Ti(salen)$_x$** (x= 0.05, 0.07, 0.09, 0.11). Their representative structure was shown in Chart S1. **HO-SiO_2-*IL*-Ti(salen)$_{0.05}$**: FT-IR: γ_{max}/cm^{-1}: 3441, 2972, 2926, 2871, 1648, 1547, 1520, 1462, 1109, 807, 620, 472. Titanium content: 0.05 mmol/g. **HO-SiO_2-*IL*-Ti(salen)$_{0.07}$**: FT-IR: γ_{max}/cm^{-1}: 3420, 3292, 3973, 3923, 2871, 1643, 1550, 1459, 1382, 1321, 1100, 941, 805, 690, 621, 468. Titanium content: 0.07 mmol/g. **HO-SiO_2-*IL*-Ti(salen)$_{0.09}$**: FT-IR: γ_{max}/cm^{-1}: 3420, 3128, 2954, 2853, 2360, 1643, 1541, 1455, 1097, 939, 867, 805, 691, 621, 466. Titanium content: 0.09 mmol/g. **HO-SiO_2-*IL*-Ti(salen)$_{0.11}$**: FT-IR: γ_{max}/cm^{-1}: 3420, 2970, 2920, 1643, 1542, 1458, 1385, 1100, 956, 805, 621, 467. Titanium content: 0.11 mmol/g.

Selectively labeling ***HO-SiO_2-IL-Ti(salen)$_{0.07}$*** *with Pd NPs.* To confirm the Janus characteristic of obtained **HO-SiO_2-*IL*-Ti(salen)$_x$**, Pd NPs was used to selectively label one side of typical **HO-SiO_2-*IL*-Ti(salen)$_{0.07}$** surface. Amino groups were introduced to the hydroxyl side of the silica JNPs in advance to absorb the Pd NPs *via* electrostatic interaction, based on affiliation between

the Pd NPs and amine groups. **HO-SiO_2-*IL*-Ti(salen)**$_{0.07}$ was dispersed in a methanol solution (5.0 mL) containing (3-aminopropyl) triethoxysilane (0.2 mmol, 0.04 g), and incubated at 75 °C and 150 rpm for 12 h, leading to the formation of amino-modified JNPs of **NH_2-SiO_2-*IL*-Ti(salen)**$_{0.07}$. A methanol solution (20 mL) containing the resulting amino-modified silica JNPs (0.2 g) was mixed with an aqueous solution containing $PdCl_2$ (28.3 mL, 0.01 M) under vigorous stirring. Lysine (20 mL of aqueous solution, 0.53 M) was then added dropwise within 30 min, and followed by the addition of $NaBH_4$ (10 mL of aqueous solution, 0.35 M). After stirring for 30 min at room temperature, Pd-labeled JNPs were collected by centrifugation (5000 rpm, 20 min), washed with ethanol three times, and then dried under vacuum for subsequent experiments.

1.5 Preparation of *IL*-free counterpart of **HO-SiO_2-Ti(salen)**$_{0.07}$ (where 0.07 represented the titanium content in samples)

For comparison, a *IL*-free counterpart of **HO-SiO_2-Ti(salen)**$_{0.07}$ (Chart S1), in which Ti(salen) units were directly located on the hemispheres of SiO_2 nanoparticles through an alkyl linker, was prepared as the control catalyst. The preparation procedure was similar to that of **HO-SiO_2-*IL*-Ti(salen)**$_{0.07}$, except for the use of $(C_2H_5O)_3$Si-Ti(salen) instead of $(C_2H_5O)_3$Si-*IL*-Ti(salen) during silylation. FT-IR: γ_{max}/cm^{-1} 3420, 2924, 2856, 1643, 1547, 1517, 1462, 1388, 1100, 955, 805, 669, 469. Titanium content: 0.07 mmol/g.

1.6 Preparation of uniform counterpart of **SiO_2-*IL*-Ti(salen)**

To investigate the "Janus effect" of **SiO_2-*IL*-Ti(salen)**, the uniform counterpart of **SiO_2-*IL*-Ti(salen)** (Chart S1), in which Ti(salen) was are uniform distributed on the surface of SiO_2 nanoparticles through IL linker, was prepared as the other control catalyst. Bare SiO_2-OH nanoparticulars (0.2 g) was incubated with $(C_2H_3O)_3$Si-*IL*-Ti(salen) (0.2 mmol, 0.2 g) in methanol

(20 mL) at 25 °C under 100 rpm for 12 h. During the procedure, the abundant surface hydroxyl groups (–OH) of SiO_2-OH were silylated with $(C_2H_5O)_3$Si-*IL*/Ti(salen). Removal of the unreacted $(C_2H_3O)_3$Si-*IL*-Ti(salen) afforded the **SiO_2-*IL*-Ti(salen)**. FT-IR (KBr): γ_{max}/cm^{-1}: 2954, 1643, 1455, 1442, 1109, 940, 805, 692, 621, 466. Titanium content: 0.12 mmol/g.

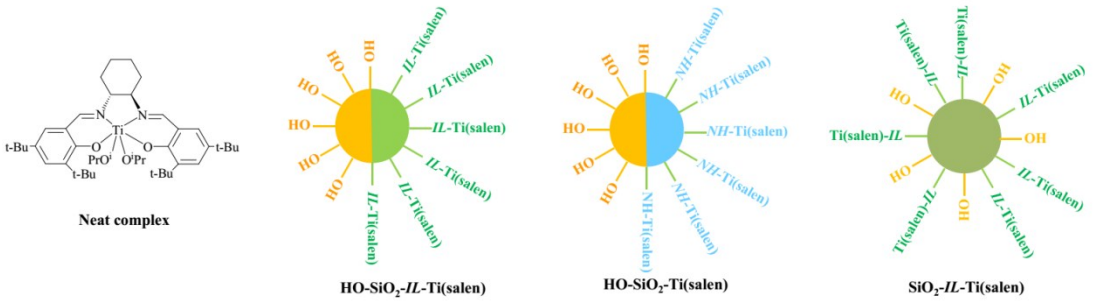

Chart S1 The representative structures of neat complex, **HO-SiO_2-*IL*-Ti(salen)**, **HO-SiO_2-Ti(salen),** and **SiO_2-*IL*-Ti(salen)**.

2. Characterization of **HO-SiO_2-*IL*-Ti(salen)$_x$ (x= 0.05, 0.07, 0.09, 0.11), HO-SiO_2-Ti(salen)$_{0.07}$,** and **SiO_2-*IL*-Ti(salen)**

2.1 FT-IR

Partially coating chiral salen Ti^{IV} complex on SiO_2 surface through an IL linker was confirmed by FT-IR spectroscopy. Fig. S1 shows the FT-IR spectra of **HO-SiO_2-*IL*-Ti(salen)$_{0.07}$** and **HO-SiO_2-Ti(salen)$_{0.07}$**, as well as the **HO-SiO_2-Ti(salen)$_{0.07}$,** pristine SiO_2-OH nanoparticles and **SiO_2-*IL*-Ti(salen)** for comparison. Pristine SiO_2-OH nanoparticles showed distinct characteristic bands at 807, 1616 and 3420 cm^{-1}, which was assigned to the skeletal vibrations of Si-C, Si-O and O-H groups, respectively (Fig. S1a).[7] Upon modification with $(C_2H_3O)_3$Si-*IL*-Ti(salen), the O-H stretching vibration (at 3420 cm^{-1}) disappeared (Fig. S1b).[8] This could be interpreted as evidence that the hydroxyl groups participated in silylation with the *IL*/Ti(salen)-containing organosiloxane.

As a result, chiral salen Ti^{IV} complex was grafted on SiO_2 surface through a flexible IL linker. Indeed, the FT-IR spectrum of **SiO_2-*IL*-Ti(salen)** exhibited the stretching vibrations of C=N in Ti(salen) (at 1648 cm^{-1}) and imidazole ring in IL moiety (at 622 cm^{-1}).[3,9] While, the O-H stretching vibration (at 3420 cm^{-1}) was present in the FT-IR spectrum of **HO-SiO_2-*IL*-Ti(salen)$_{0.07}$**, although its intensity was significantly decreased (Fig. S1c). It was evidence for the partial modification of SiO_2 surface with $(C_2H_3O)_3$Si-*IL*-Ti(salen). Logically, the hydroxyl group buried in wax was intact during the silylation process. The region-selective modification endowed **HO-SiO_2-*IL*-Ti(salen)$_x$** with not only catalytic reactivity, but also interfacial activity, which were crucial in Pickering interfacial catalysis. *IL*-free counterpart of **HO-SiO_2-Ti(salen)$_{0.07}$** exhibited similar FT-IR spectrum to **HO-SiO_2-*IL*-Ti(salen)$_{0.07}$**, except for the absence of the characteristic stretching vibrations of the imidazole ring at 621 cm^{-1} (Fig. S1d *vs*. S1c).[3,9] The results correlate with the Janus geometry of **HO-SiO_2-Ti(salen)$_{0.07}$** and the inexistence of imidazolium-based IL linker. Notably, the active species of Ti(salen) was intact during the grafting as its characteristic bands in SiO_2-supported samples are identical to those in neat complex (Fig. S1b-d *vs.* S1e).

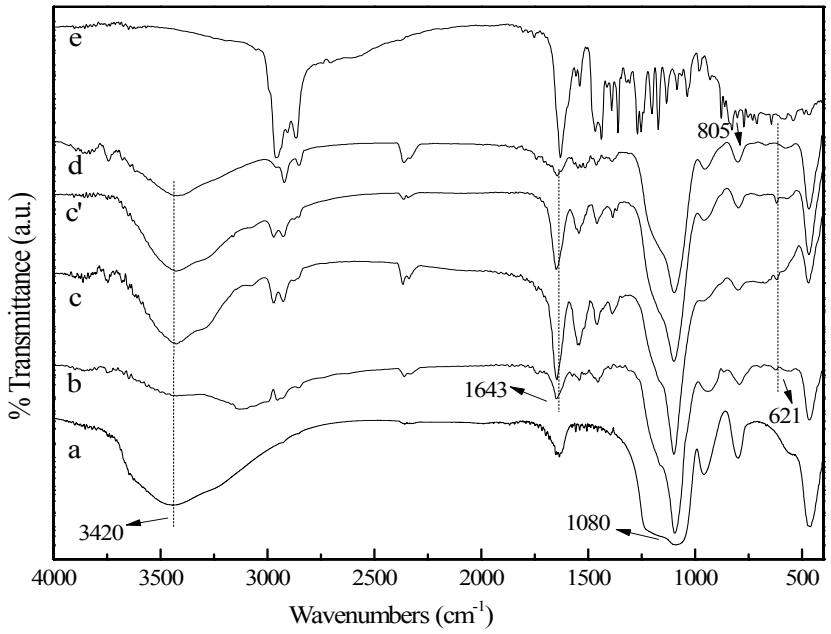

Fig. S1 FT-IR spectra of bare SiO_2-OH (a), **SiO_2-*IL*-Ti(salen)** (b), **HO-SiO_2-*IL*-Ti(salen)$_{0.07}$** (c), the recovered **HO-SiO_2-*IL*-Ti(salen)$_{0.07}$** after the 7th reuse (c′), **HO-SiO_2-Ti(salen)$_{0.07}$** (d), and neat complex (e).

2.2 TEM

TEM images were used to obtain information on the particle size and morphology of as-prepared samples of SiO_2-OH, **HO-SiO_2-*IL*-Ti(salen)$_x$** (x=0.05, 0.07, 0.09, 0.11), **SiO_2-*IL*-Ti(salen)** and **HO-SiO_2-Ti(salen)$_{0.07}$**, as shown in Fig. S2. Particles with an approximately spherical shape and average diameter of *ca.* 40 nm were observed on the image of SiO_2-OH (Fig. S2A). The size and morphology did not significantly change after anchoring the Ti(salen) moiety onto the partial silica surface using an imidazolium-based IL linker (Fig. S2B-E). This finding suggested that the silica core was intact during immobilization and that the functional reaction occurred only on the particle surface. To confirm the Janus characteristic of **HO-SiO_2-*IL*-Ti(salen)$_x$**, we further modified the hydroxyl side of typical **HO-SiO_2-*IL*-Ti(salen)$_{0.07}$** with 3-aminopropyltriethoxysilane through silylation, and labelled the amino with Pd nanoparticles (NPs). Indeed, the Pd NPs mainly adsorbed on one side of the silica JNPs in the TEM image of Pd-labelled sample (Fig. S2H). The nanometer size, together with asymmetric dispersion of catalytically active centers on the surface, made **HO-SiO_2-*IL*-Ti(salen)$_x$** efficient in aqueous asymmetric sulfoxidation. Additionally, uniform **SiO_2-*IL*-Ti(salen)** (Fig. S2F) and *IL*-free **HO-SiO_2-Ti(salen)$_{0.07}$** (Fig. S2G) also showed the approximately spherical particles with an average particle diameter of *ca.* 40 nm in the corresponding TEM image.

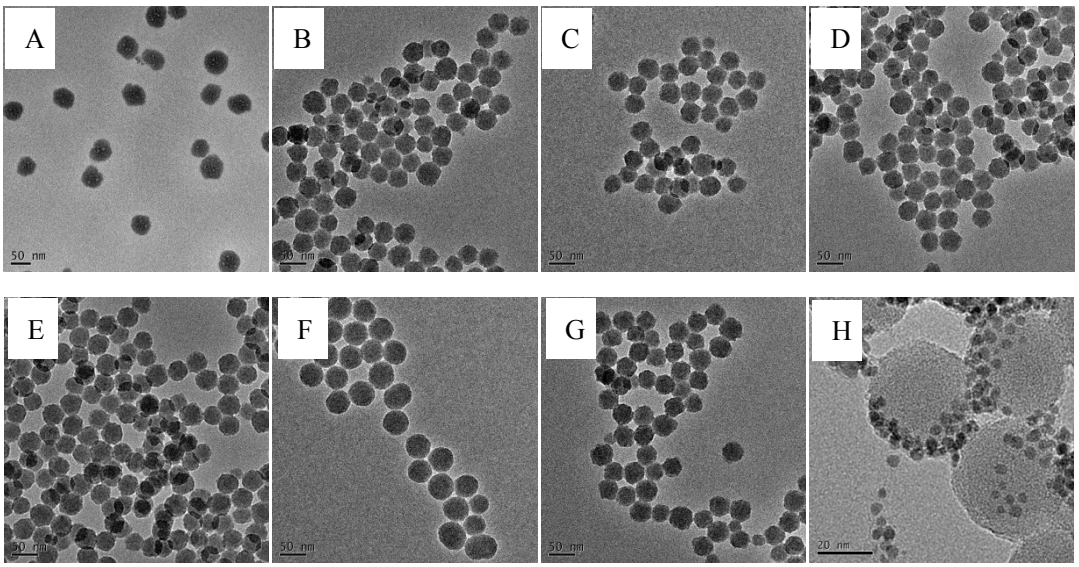

Fig. S2 TEM images of SiO_2-OH (A), **HO-SiO_2-*IL*-Ti(salen)$_{0.05}$** (B), **HO-SiO_2-*IL*-Ti(salen)$_{0.07}$** (C), **HO-SiO_2-*IL*-Ti(salen)$_{0.09}$** (D), **HO-SiO_2-*IL*-Ti(salen)$_{0.11}$** (E), **SiO_2-*IL*-Ti(salen)** (F), **HO-SiO_2-Ti(salen)**$_{0.07}$ (G) and Pd NPs-labeled **HO-SiO_2-*IL*-Ti(salen)$_{0.07}$** (H) in methanol.

2.3 Particle size distribution analysis

DLS was used to further determine the change in nanoparticles size after modification, as shown in Fig. S3. Bare SiO_2-OH showed the mean hydrodynamic diameter of 141 nm (Fig. S3A). Modification of *IL*-Ti(salen) moiety on the surface resulted in an increase in the hydrodynamic diameter. Logically, the more *IL*-Ti(salen) moiety on SiO_2-OH surface, the larger the nanoparticles size became. Indeed, JNPs with x= 0.05, 0.07, 0.09, and 0.11 mmol/g gave hydrodynamic diameter of *ca.* 190, 225, 295, and 325 nm, respectively (Fig. S3B). When the silica surface was uniformed covered by *IL*-Ti(salen), the hydrodynamic diameter was up to 342 nm (Fig. S3C). *IL*-free counterpart of **HO-SiO_2-Ti(salen)**$_{0.07}$ showed a smaller average hydrodynamic diameter (*ca.* 209 nm) than **HO-SiO_2-*IL*-Ti(salen)**$_{0.07}$ (225 nm) (Fig. S3D *vs.* S3B). Furthermore, we noticed that the sizes for nanoparticles determined by DLS were larger than from TEM,

probably due to the presence of a solvation layer on the particles.

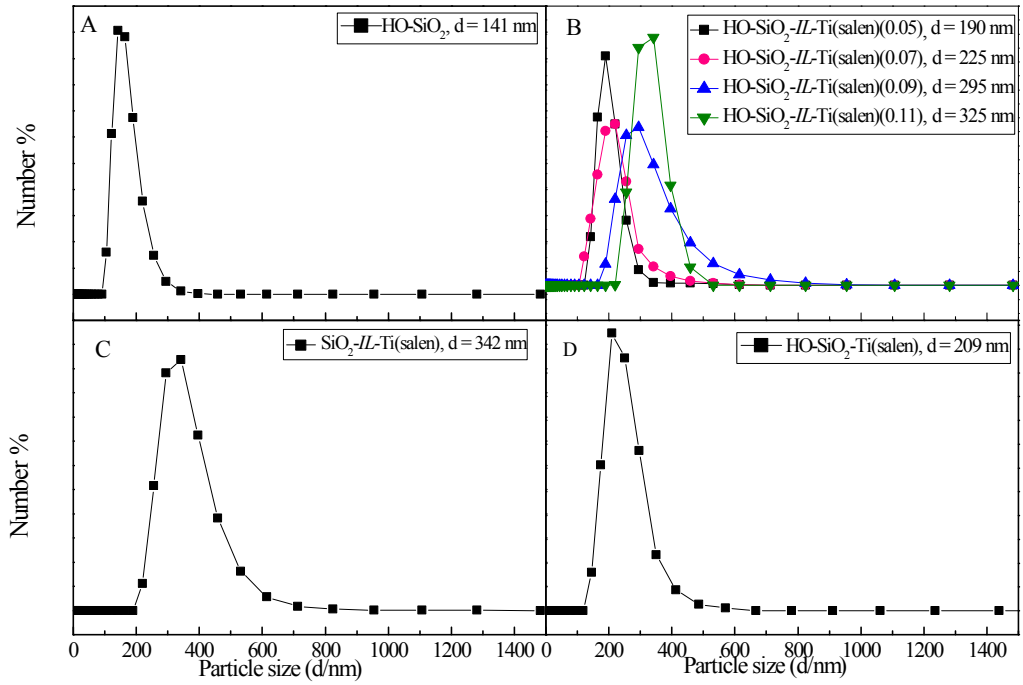

Fig. S3 Size distribution of SiO_2-OH (A), **HO-SiO_2-*IL*-Ti(salen)$_x$** (x= 0.05, 0.07, 0.09, 0.11) (B), **SiO_2-*IL*-Ti(salen)** (C) and **HO-SiO_2-Ti(salen)$_{0.07}$** (D) in methanol at a concentration of 1.0 mg mL^{-1} at room temperature.

2.4 Pickering emulsions stabilized by **HO-SiO_2-*IL*-Ti(salen)$_x$**

Successful creation of emulsion can be confirmed by optical micrographs, as shown in Fig. S4. Spherical emulsions droplets with a controlled size at the micrometer scale were observed in the Pickering emulsion stabilized by **HO-SiO_2-*IL*-Ti(salen)$_x$**. The average size of these droplets was varied with their degree of hydrophobization. **HO-SiO_2-*IL*-Ti(salen)$_{0.07}$** gave the smallest emulsion droplets with diameter of *ca.* 12 μm (Fig. S4B). Further enhancing or reducing the Ti(salen) content on JNPs led to the increased emulsion droplets size accordingly (Fig. S4A, S4C, and S4D *vs.* S4B). A possible explanation might be that the JNPs became more hydrophobic with the Ti(salen) increasing, penetrating more deeply into the oil phase.[6] It thus reduced the surface

exposed to continuous water phase. For **HO-SiO_2-*IL*-Ti(salen)$_x$** (x= 0.05 and 0.07), the available particles with larger hydrophilic surface might be sufficient to fully cover the droplet interfaces. In this case, the droplet size reduced with increasing Ti(salen) content as a consequence of enhanced interparticle hydrophobic effect (Fig. S4B *vs.* S4A).[9] When the hydrophilic area decreased beyond a critical value, the particles available were initially insufficient to fully cover the oil-water interfaces, as the case of **HO-SiO_2-*IL*-Ti(salen)$_x$** (x= 0.09 and 0.11). As a result, the emulsion droplets underwent a "limited coalescence" process to minimize the free energy until the particle layer at interface was dense enough to prevent further coalescence.[9, 10] The extent of coalescence was increased with the degree of hydrophobization of JNPs, which increased the droplets size accordingly (Fig. S4D *vs.* S4C *vs.* S4B). The preferred sizes of emulsion droplets determined the interfacial area of corresponding Pickering emulsion, which hence affected the interfacial mass transfer in Pickering interfacial catalysis.[11] Benefiting from the Janus characteristic, **HO-SiO_2-Ti(salen)$_{0.07}$** as an emulsifier also gave the stable emulsions with droplets diameter of *ca.* 65 μm (Fig. S4F). Different from JNPs-stabilized emulsions which are thermodynamically stable, the Pickering emulsions stabilized with uniform **SiO_2-*IL*-Ti(salen)** particles are only kinetically stable and thus can undergo destabilization (Fig. S4E).[8] Stable Pickering emulsions together with controllable interfacial area made **HO-SiO_2-*IL*-Ti(salen)$_x$** the desirable Pickering interfacial catalysts for asymmetric sulfoxidation in water.

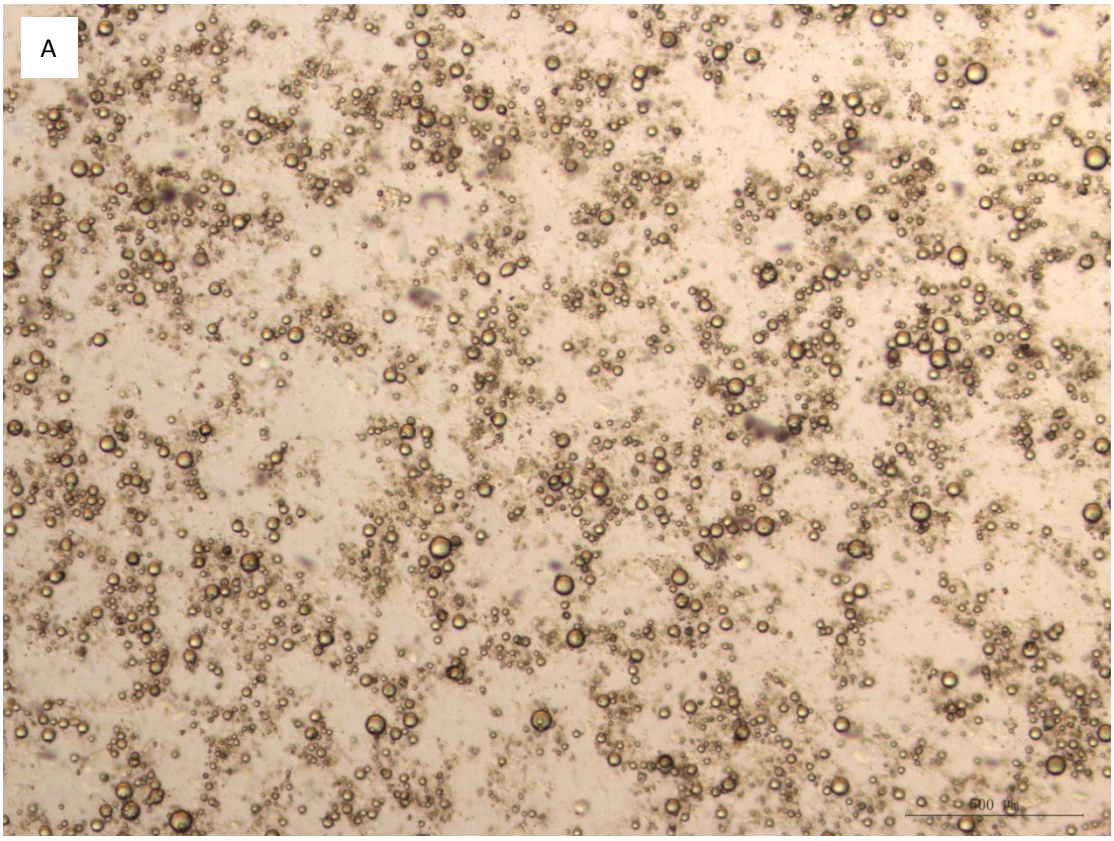
A
500 µm

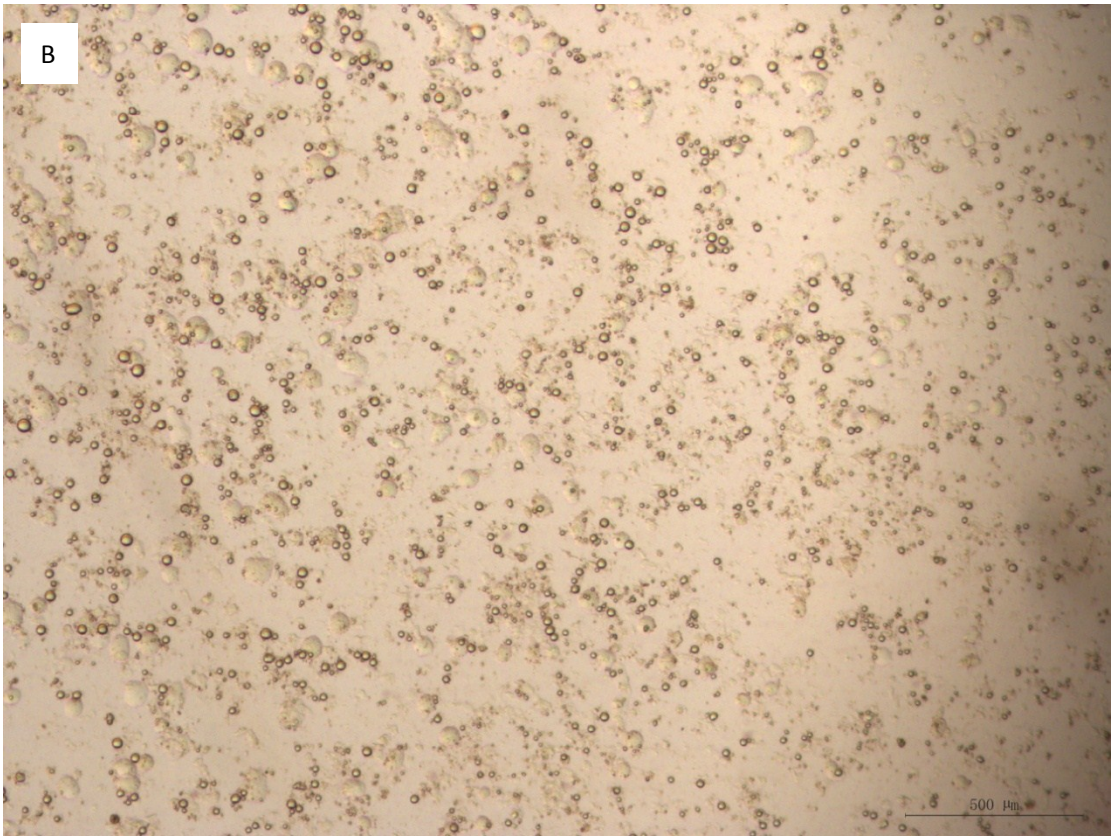
B
500 µm

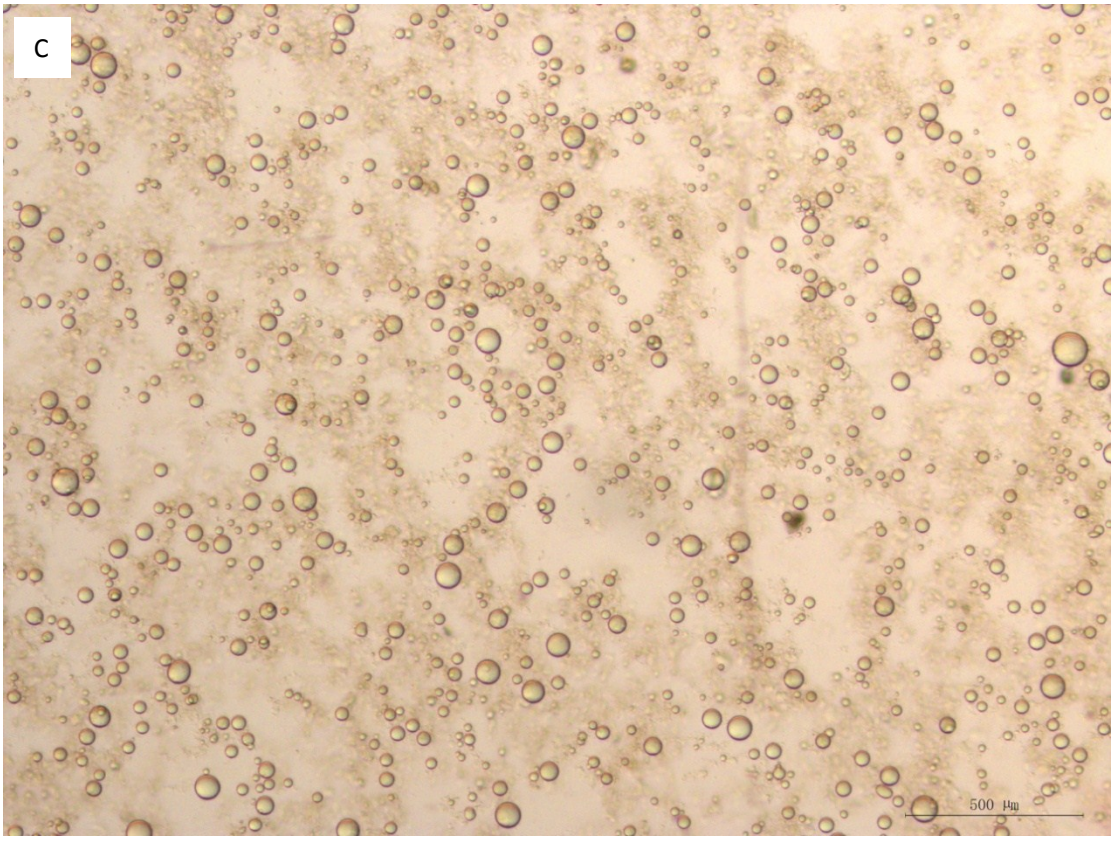
C
500 µm

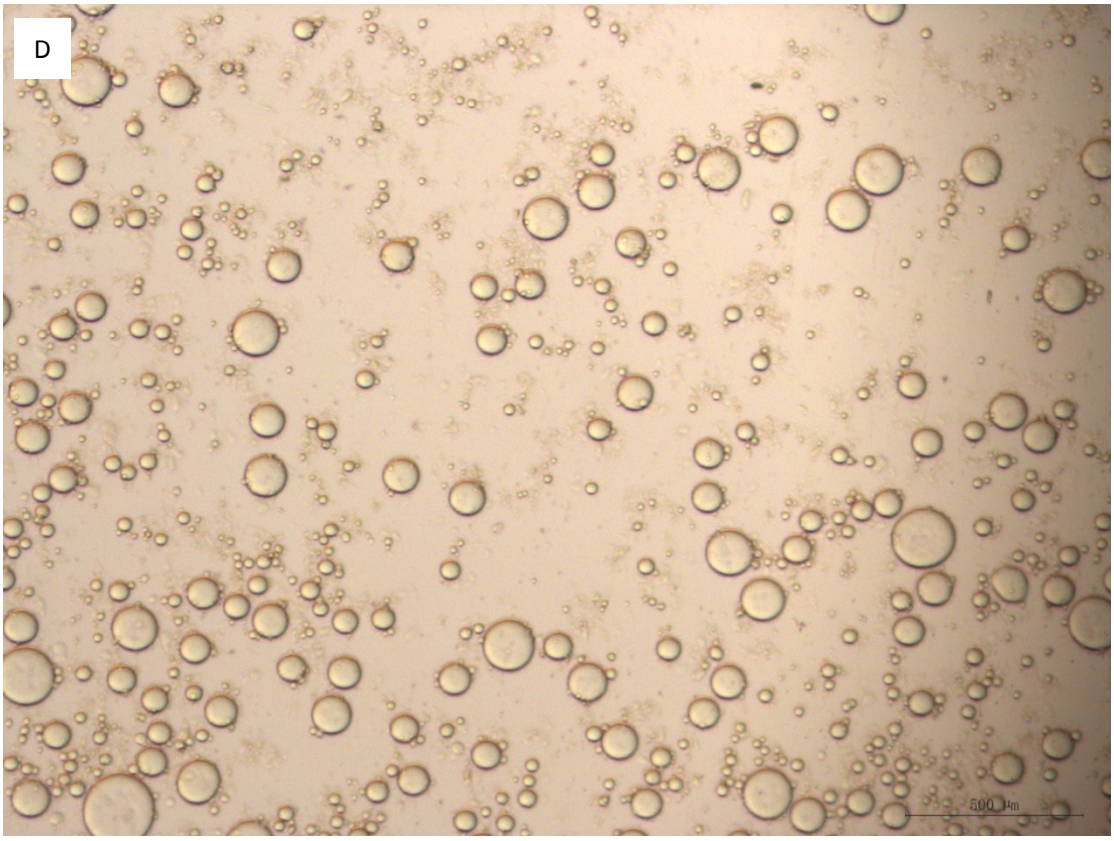
D
500 µm

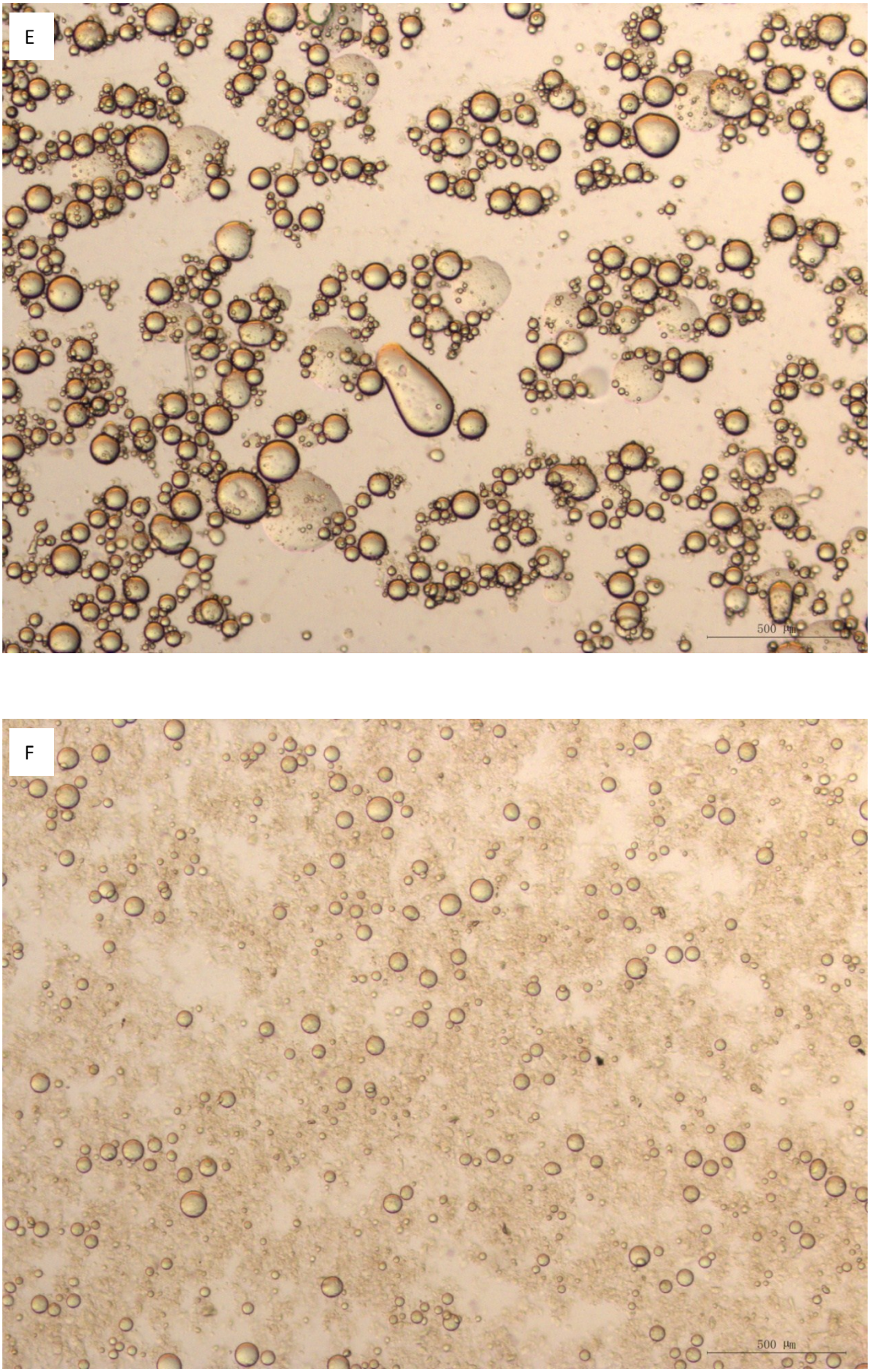

Fig. S4 Optical microscopy image of the sulfide-in-H_2O emulsions stabilized **HO-SiO_2-*IL*-**

Ti(salen)$_{0.05}$ (A), **HO-SiO$_2$-*IL*-Ti(salen)$_{0.07}$** (B), **HO-SiO$_2$-*IL*-Ti(salen)$_{0.09}$** (C), **HO-SiO$_2$-*IL*-Ti(salen)$_{0.011}$** (D), **SiO$_2$- *IL*-Ti(salen)** (E), and **HO-SiO$_2$-Ti(salen)$_{0.07}$** (F). Chiral salen Ti^{IV} catalyst (0.1 g) and methyl phenyl sulfide (0.2 mL) were suspended in water (1 mL) and stirred (10 000 rpm) for 10 min, before the images were taken.

3. The evaluation of catalytic activity of **HO-SiO$_2$-*IL*-Ti(salen)$_x$** in asymmetric sulfoxidation in water.

3.1 General procedure for asymmetric sulfoxidation in water

Ti^{IV}-based catalyst (1.25 mol% of substrate) was stirred with sulfides (0.5 mmol) in deionized water (1 mL) at 25 °C. H_2O_2 (30 *wt.*%, 0.6 mmol) was then added dropwise over 15 min. The resulting mixture was stirred at 25 °C. Reaction progress was monitored on GC. After the reaction, the catalyst was recovered by centrifugation, washed with ethyl acetate, dried in a vacuum, and finally recharged with fresh substrate and oxidant for the next catalytic cycle. The reaction solution was extracted with ethyl acetate (3 × 4 mL). Combined organic layer was dried over anhydrous sodium sulfate and was concentrated in vacuo. Notably, although ethyl acetate was used to extract a small amount of sulfide in the present work, this approach should be redundant in large-scale industrial processes, in which the oily product phase can be directly separated from water after catalyst removal. Further purification of the residue by chromatography on silica gel (petroleum ether/ethyl acetate, 1.5: 1) afforded chiral sulfoxides. The depurated sulfoxides have been identified by ^{1}H NMR spectra. Ee values of the products were determined by HPLC analysis using the Daicel chiralpak AD columns.

Phenyl methyl sulfoxide: The product has been identified by ^{1}H and ^{13}C NMR spectra (see Fig.

S5 and S6). ^{1}H NMR ($CDCl_3$, 500 MHz): δ (ppm): 7.65-7.64 (m, 2 H, Ar*H*), 7.52-7.49 (m, 3 H, Ar*H*), 2.71 (s, 3 H, S-CH_3), ^{13}C NMR ($CDCl_3$, 125 MHz): δ (ppm): 43.90 (*C*H_3), 123.53, 129.38, 131.09, 145.57 (Ar*C*). Chemoselectivity was determined by GC, nitrogen was used as the carrier gas with a flow of 40 mL/min, injector temperature and detector temperature were 250 °C, column temperature was 180 °C, $t_{phenyl\ methyl\ sulfoxide}$ = 2.1 min; ee value was determined by HPLC (*i*-PrOH/*n*-hexane = 2.5: 7.5 (v/v)); flow rate = 1.0 mL/min; 25 °C; λ = 254 nm; major enantiomer t_R = 7.7 min, minor enantiomer t_S = 9.7 min(see Fig. S7-S10)

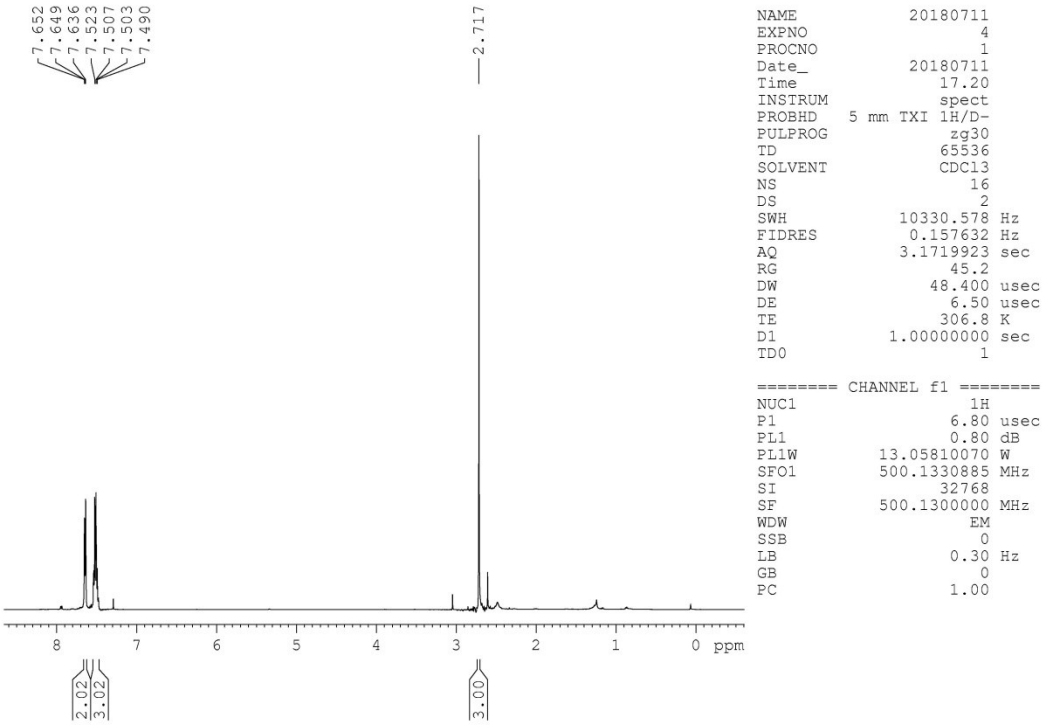

Fig. S5 ^{1}H NMR of phenyl methyl sulfoxide.

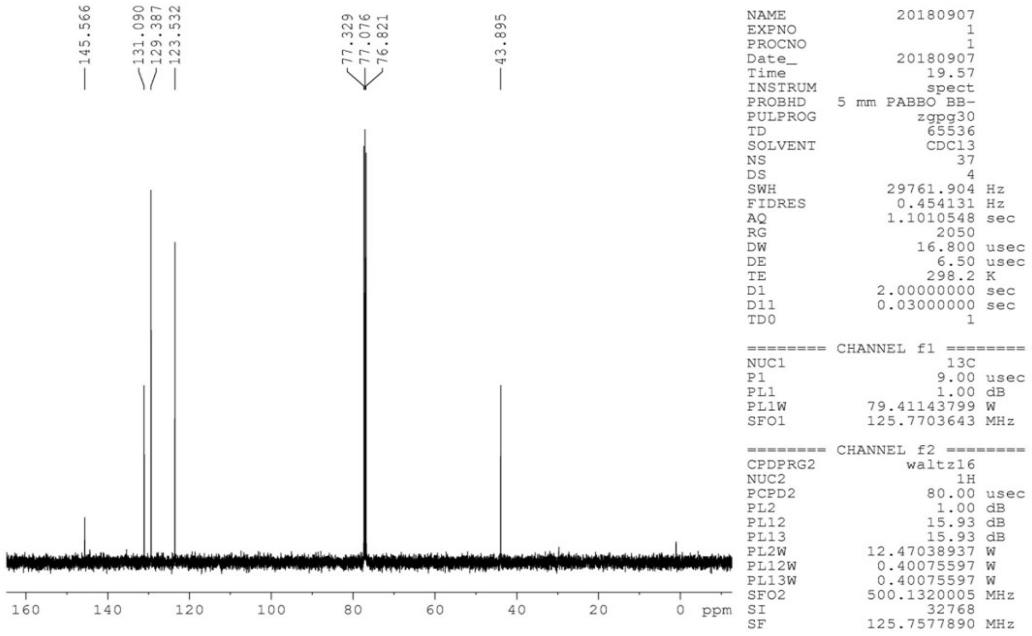

Fig. S6 ^{13}C NMR of phenyl methyl sulfoxide

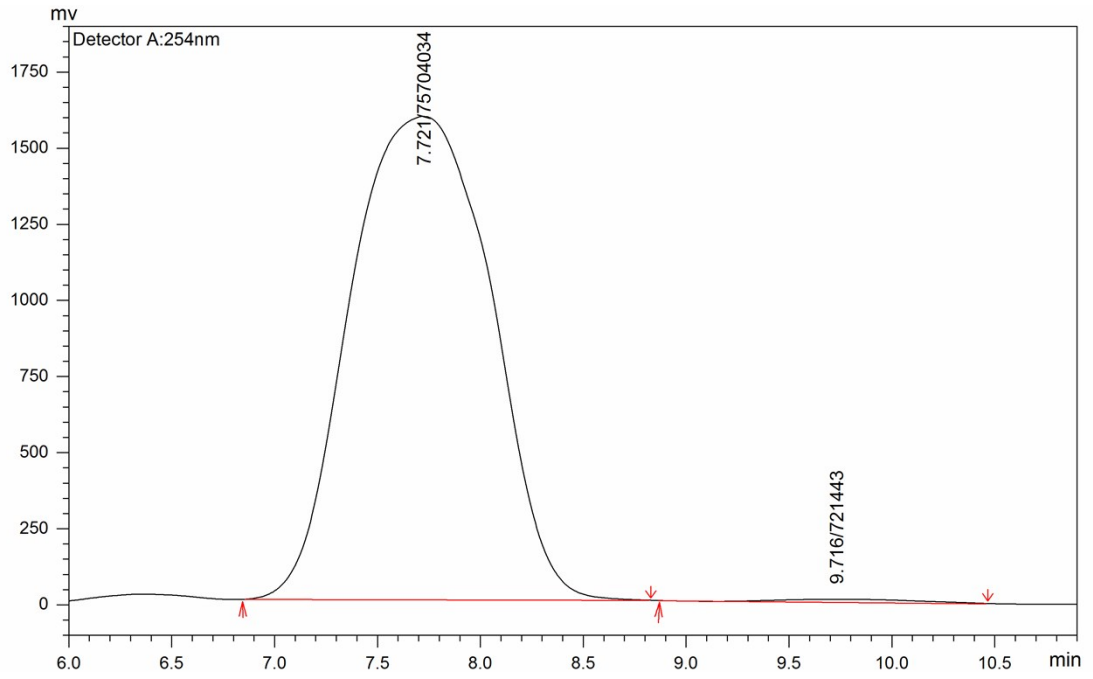

Fig. S7 HLPC of phenyl methyl sulfoxide obtained over **HO-SiO$_2$-*IL*-Ti(salen)$_{0.07}$** (ee value = 98%).

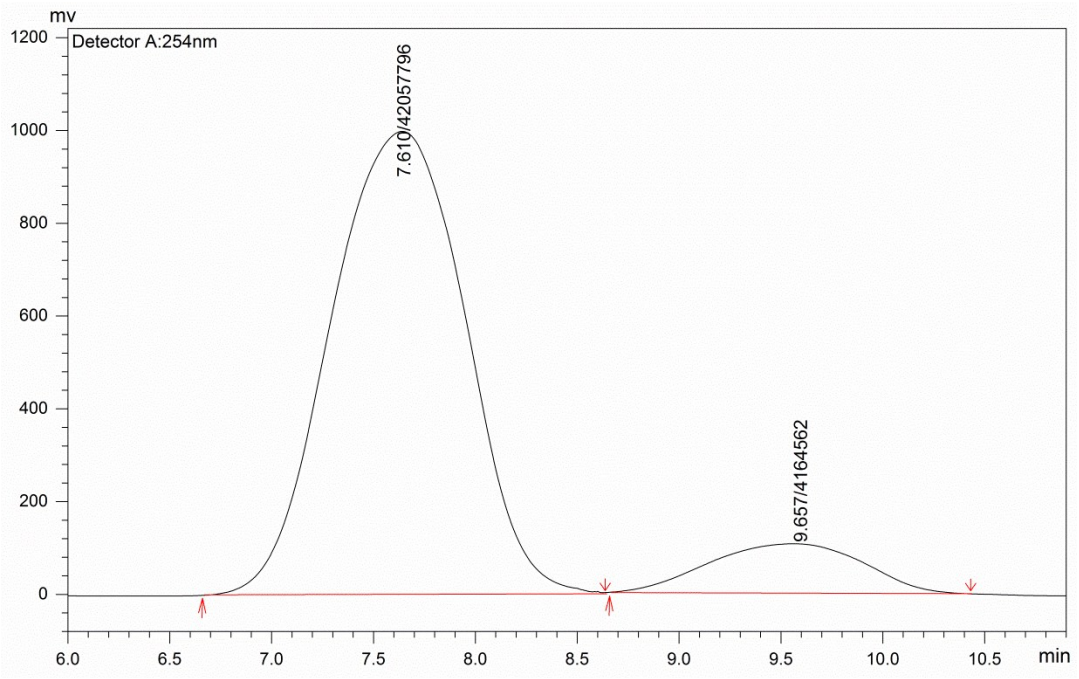

Fig. S8 HLPC of phenyl methyl sulfoxide obtained over **SiO_2-*IL*-Ti(salen)** (ee value = 82%).

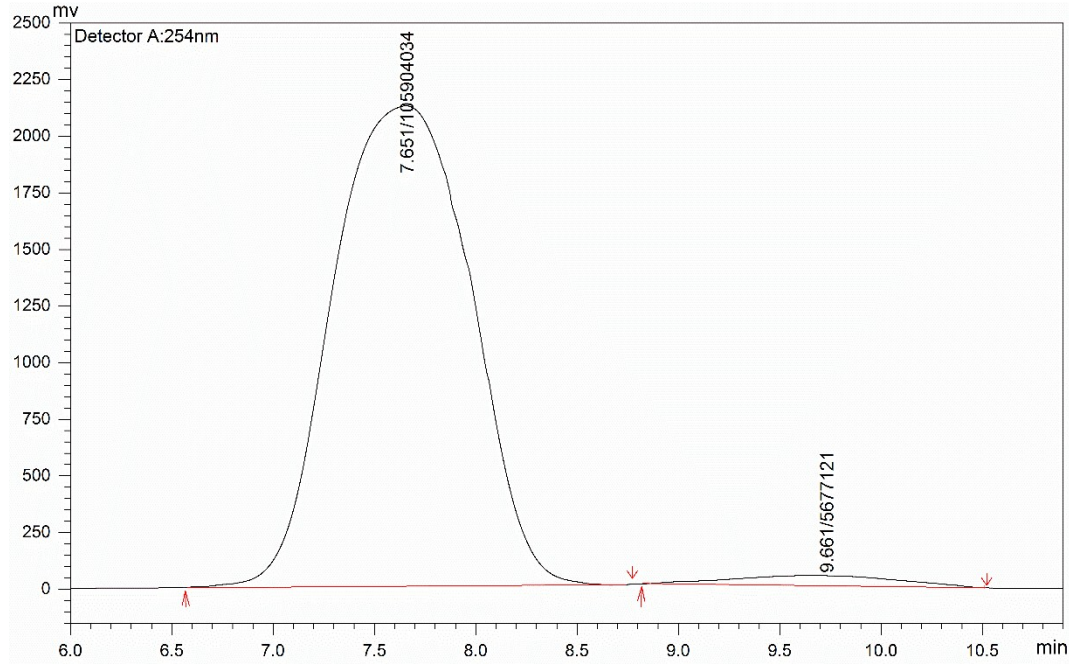

Fig. S9 HLPC of phenyl methyl sulfoxide obtained over **HO-SiO_2-Ti(salen)$_{0.07}$** (ee value = 94%)

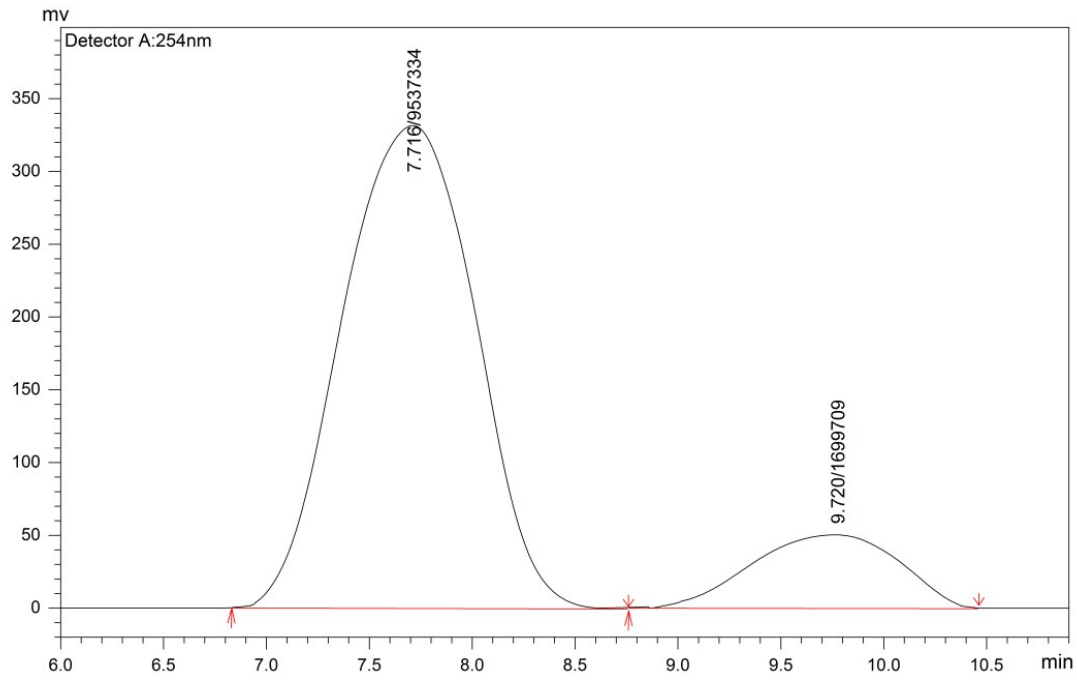

Fig. S10 HLPC of phenyl methyl sulfoxide obtained over neat complex (ee value = 70%).

Phenyl ethyl sulfoxide: The product has been identified by ^{1}H and ^{13}C NMR spectra (see Fig. S11 and S12). ^{1}H NMR ($CDCl_3$, 500 MHz): δ (ppm): 7.51-7.50 (m, 2 H, Ar*H*), 7.41-7.40 (m, 3 H, Ar*H*), 2.84-2.64 (m, 2 H, S-C*H*$_2$-CH$_3$), 1.10-1.07(m, 3 H, S-CH$_2$-C*H*$_3$). ^{13}C NMR ($CDCl_3$, 125 MHz): δ (ppm): 5.94 (*C*H$_3$), 50.27 (*C*H$_2$), 124.16, 129.13, 130.92, 143.29 (Ar*C*). Chemoselectivity was determined by GC, nitrogen was used as the carrier gas with a flow of 40 mL/min, the injector temperature and the detector temperature were 250 °C, the column temperature was 180 °C, $t_{phenyl\ ethyl\ sulfoxide}$ = 2.2 min; ee value was determined by HPLC (*i*-PrOH/*n*-hexane = 2.5: 7.5 (v/ v)); flow rate = 1.0 mL/min; 25 °C; λ = 254 nm; major enantiomer t_R = 7.0 min, minor enantiomer t_S = 8.8 min (see Fig. S13-S16).

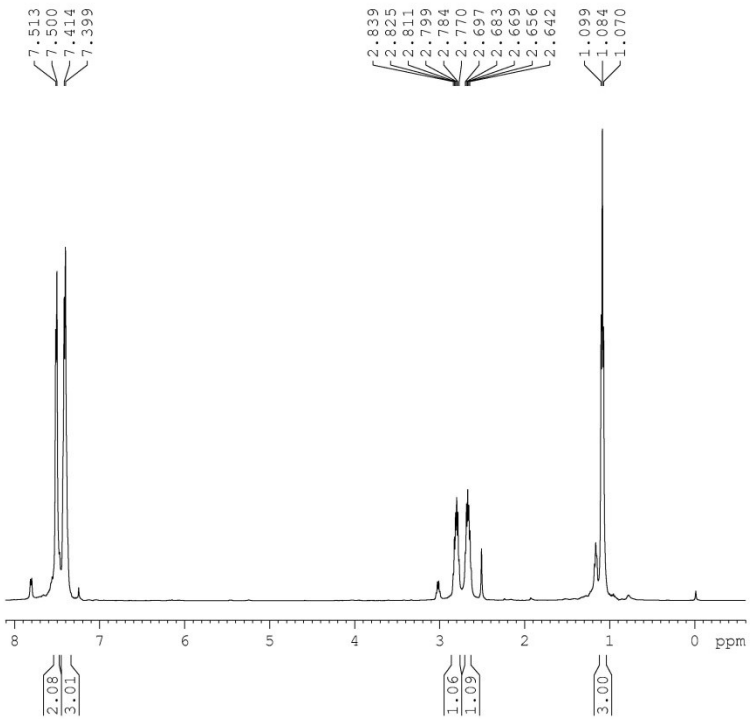


```
NAME            20180711
EXPNO                  3
PROCNO                 1
Date_           20180711
Time               17.12
INSTRUM            spect
PROBHD    5 mm TXI 1H/D-
PULPROG             zg30
TD                 65536
SOLVENT            CDCl3
NS                    16
DS                     2
SWH           10330.578 Hz
FIDRES         0.157632 Hz
AQ             3.1719923 sec
RG                  28.5
DW                48.400 usec
DE                 6.50 usec
TE                307.0 K
D1             1.00000000 sec
TD0                    1

======== CHANNEL f1 ========
NUC1                  1H
P1                 6.80 usec
PL1                0.80 dB
PL1W        13.05810070 W
SFO1       500.1330885 MHz
SI                 32768
SF         500.1300230 MHz
WDW                   EM
SSB                    0
LB                 0.30 Hz
GB                     0
PC                 1.00
```

Fig. S11 ^{1}H NMR of phenyl ethyl sulfoxide.

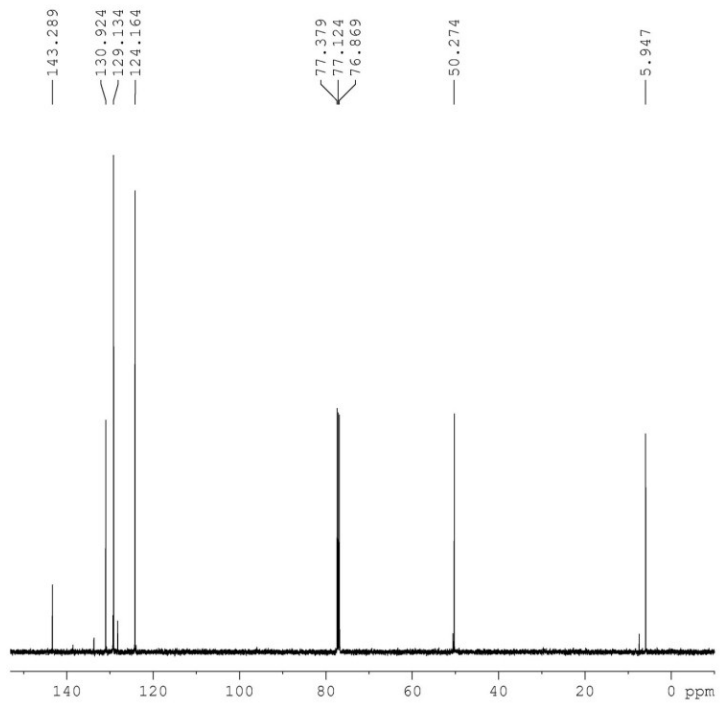


```
NAME            20180905
EXPNO                  4
PROCNO                 1
Date_           20180905
Time               18.05
INSTRUM            spect
PROBHD    5 mm PABBO BB-
PULPROG          zgpg30
TD                 65536
SOLVENT            CDCl3
NS                   158
DS                     4
SWH           29761.904 Hz
FIDRES         0.454131 Hz
AQ             1.1010548 sec
RG                  2050
DW                16.800 usec
DE                 6.50 usec
TE                299.1 K
D1             2.00000000 sec
D11            0.03000000 sec
TD0                    1

======== CHANNEL f1 ========
NUC1                 13C
P1                 9.00 usec
PL1                1.00 dB
PL1W        79.41143799 W
SFO1       125.7703643 MHz

======== CHANNEL f2 ========
CPDPRG2          waltz16
NUC2                  1H
PCPD2             80.00 usec
PL2                1.00 dB
PL12              15.93 dB
PL13              15.93 dB
PL2W        12.47038937 W
PL12W        0.40075597 W
PL13W        0.40075597 W
SFO2       500.1320005 MHz
SI                 32768
SF         125.7577890 MHz
```

Fig. S12 ^{13}C NMR of phenyl ethyl sulfoxide.

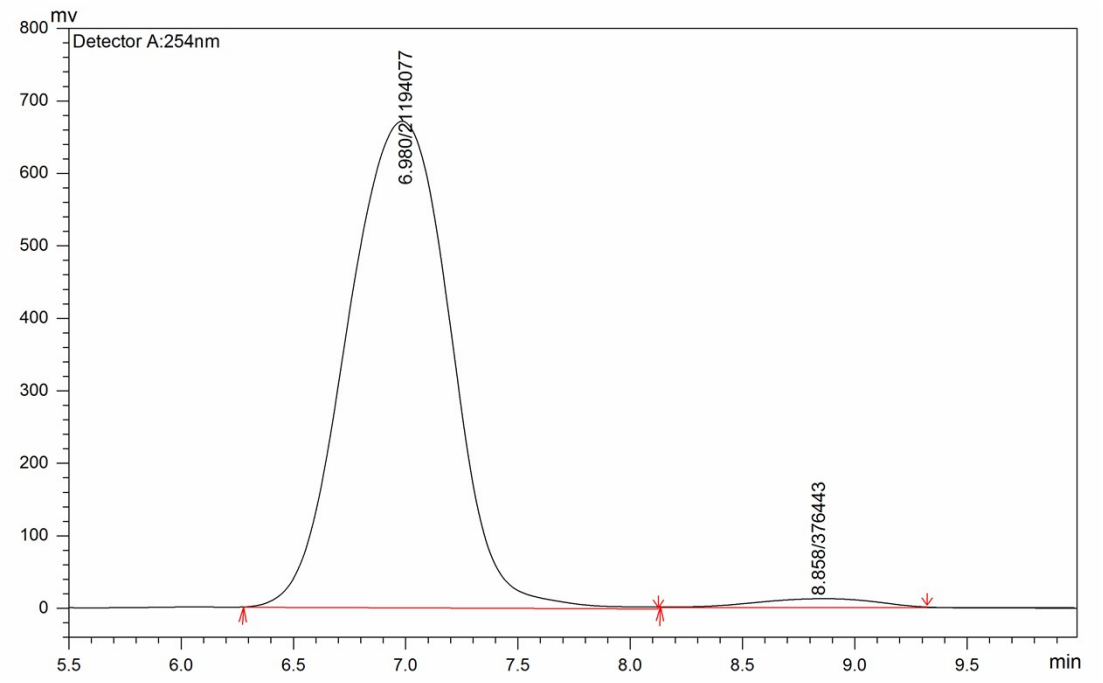

Fig. S13 HLPC of phenyl ethyl sulfoxide obtained over **HO-SiO_2-*IL*-Ti(salen)$_{0.07}$** (ee value = 97%).

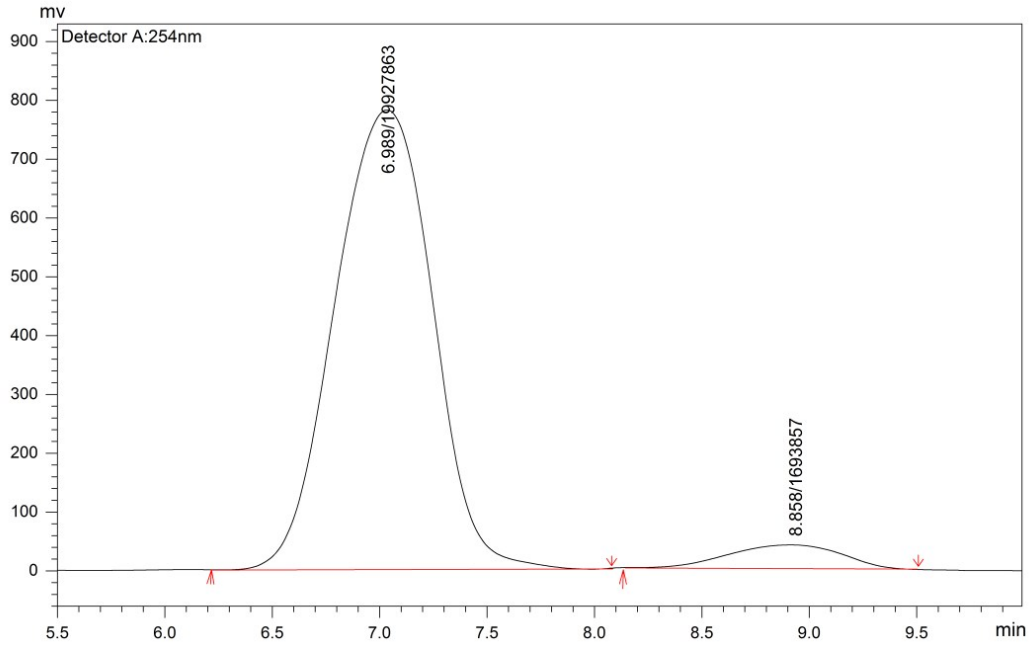

Fig. S14 HLPC of phenyl ethyl sulfoxide obtained over **SiO_2-*IL*-Ti(salen)** (ee value = 84%).

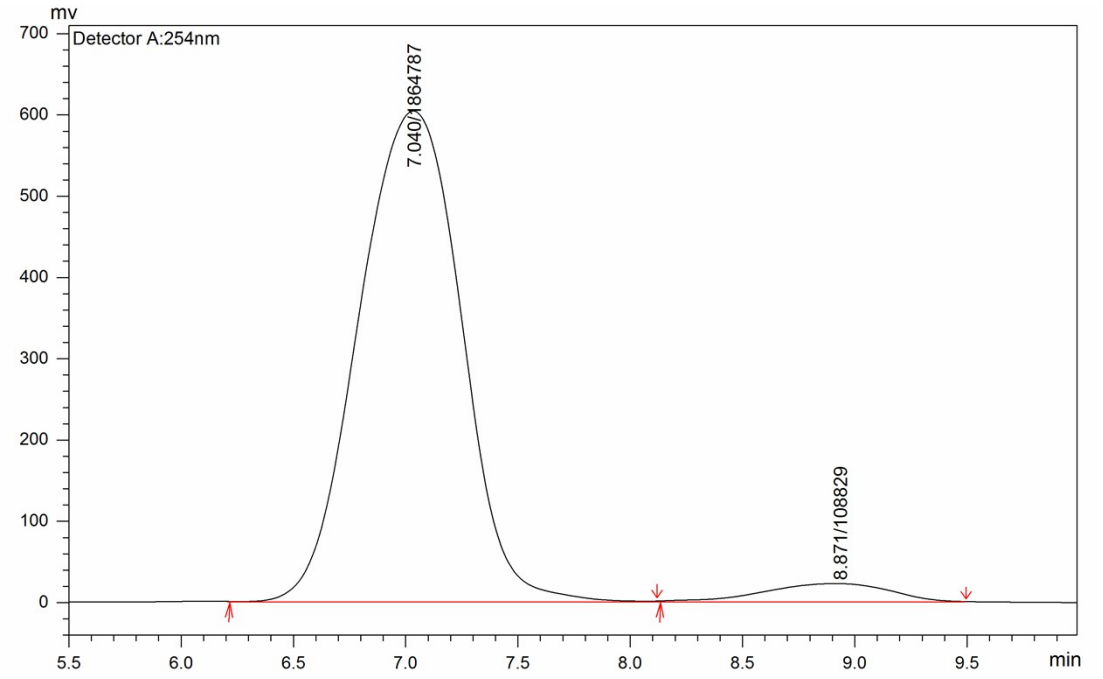

Fig. S15 HLPC of phenyl ethyl sulfoxide obtained over **HO-SiO$_2$-Ti(salen)$_{0.07}$** (ee value = 88%).

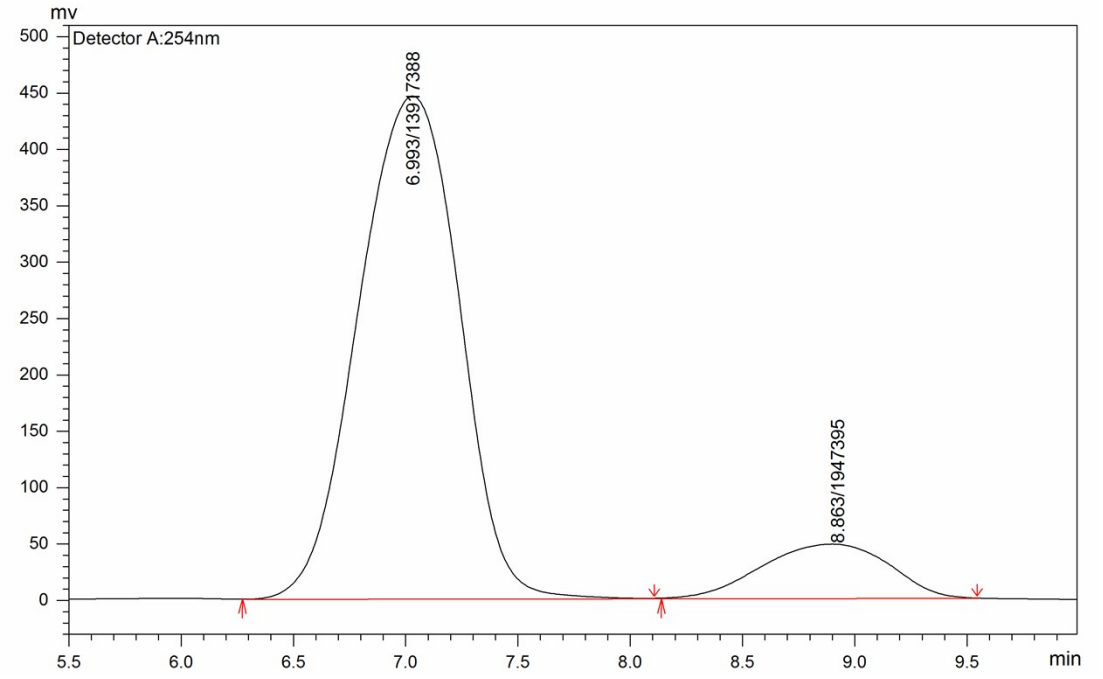

Fig. S16 HLPC of phenyl ethyl sulfoxide obtained over neat complex (ee value = 75%).

Phenyl *n*-butyl sulfoxide: The product has been identified by ^{1}H and ^{13}C NMR spectra (see Fig.

S17 and S18).[1]H NMR ($CDCl_3$, 500 MHz): δ (ppm): 7.65-7.63 (m, 2 H, Ar*H*), 7.54-7.52 (m, 3 H, Ar*H*), 2.82-2.79 (m, 2 H, S-C*H*$_2$-), 1.76-1.60 (m, 2 H, S-CH_2-C*H*$_2$-), 1.48-1.43 (m, 2 H, S-CH_2-CH_2-C*H*$_2$-), 0.95-0.92 (m, 3 H, S-CH_2-CH_2-CH_2-C*H*$_3$). [13]C NMR ($CDCl_3$, 125 MHz): δ (ppm): 13.66 (*C*H_3), 21.90 (*C*H_2), 24.16 (*C*H_2), 57.09 (*C*H_2), 124.05, 129.20, 130.93, 144.02 (Ar*C*). Chemoselectivity was determined by GC, nitrogen was used as the carrier gas with a flow of 40 mL/min, the injector temperature and the detector temperature were 250 °C, the column temperature was 180 °C, $t_{phenyl\ n\text{-}butyl\ sulfoxide}$ = 2.6 min; ee value was determined by HPLC (i-PrOH/*n*-hexane = 2.5: 7.5 (v/v)); flow rate = 1.0 mL/min; 25 °C; λ = 254 nm; major enantiomer t_R = 5.6 min , minor enantiomer t_S = 7.1 min (see Fig. S19-S22).

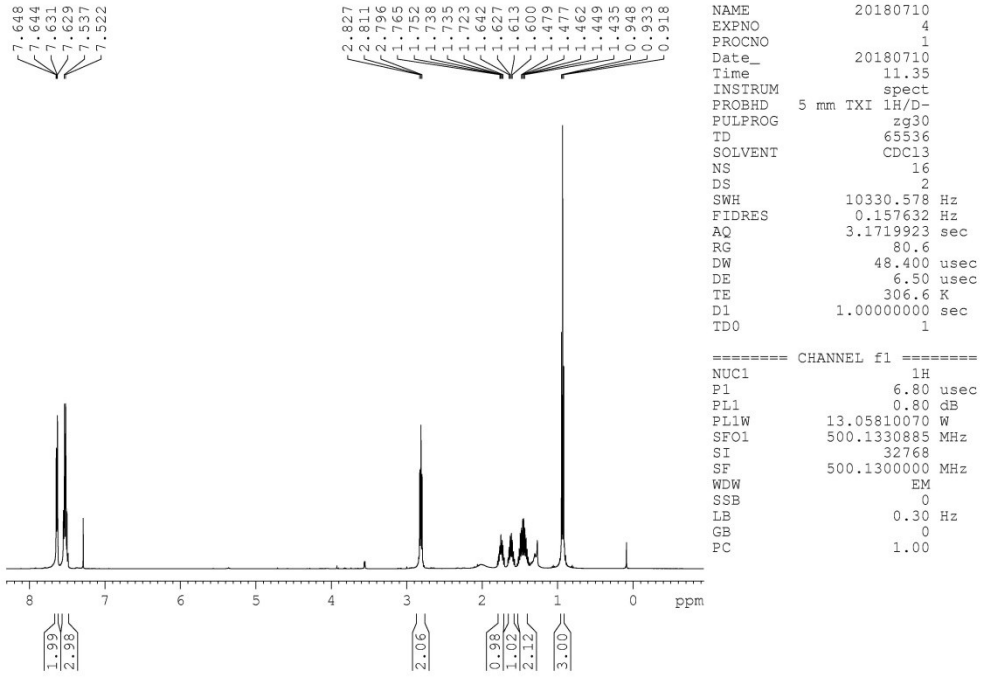

Fig. S17 [1]H NMR of phenyl *n*-butyl sulfoxide.

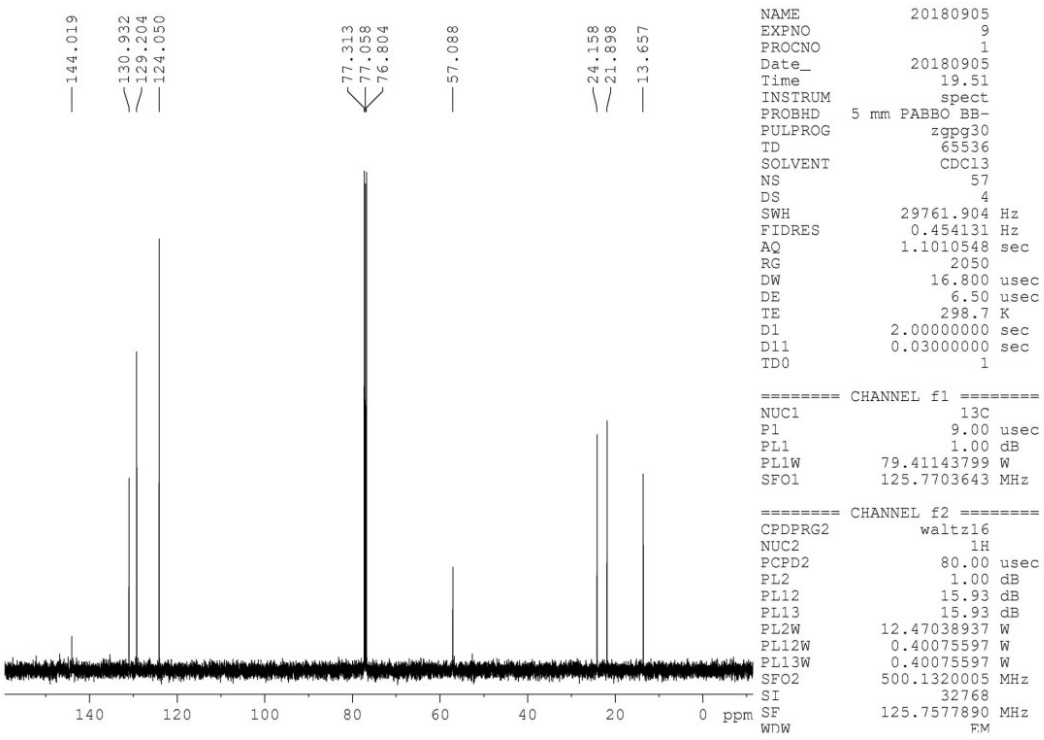

Fig. S18 ^{13}C NMR of phenyl *n*-butyl sulfoxide.

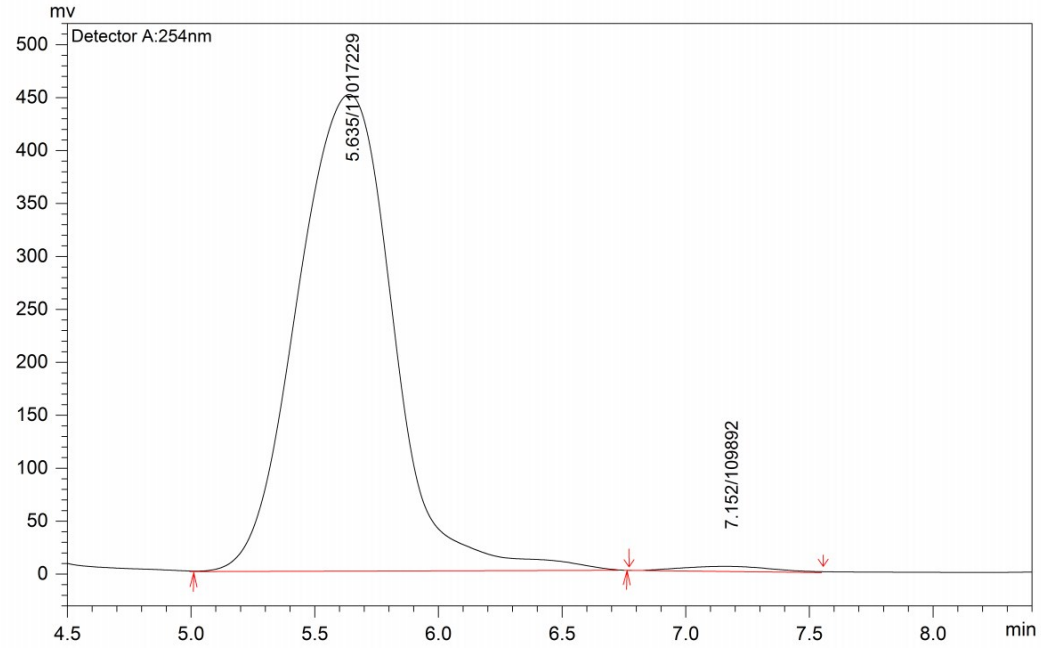

Fig. S19 HLPC of phenyl *n*-butyl sulfoxide obtained over **HO-SiO$_2$-*IL*-Ti(salen)$_{0.07}$** (ee value = 98%).

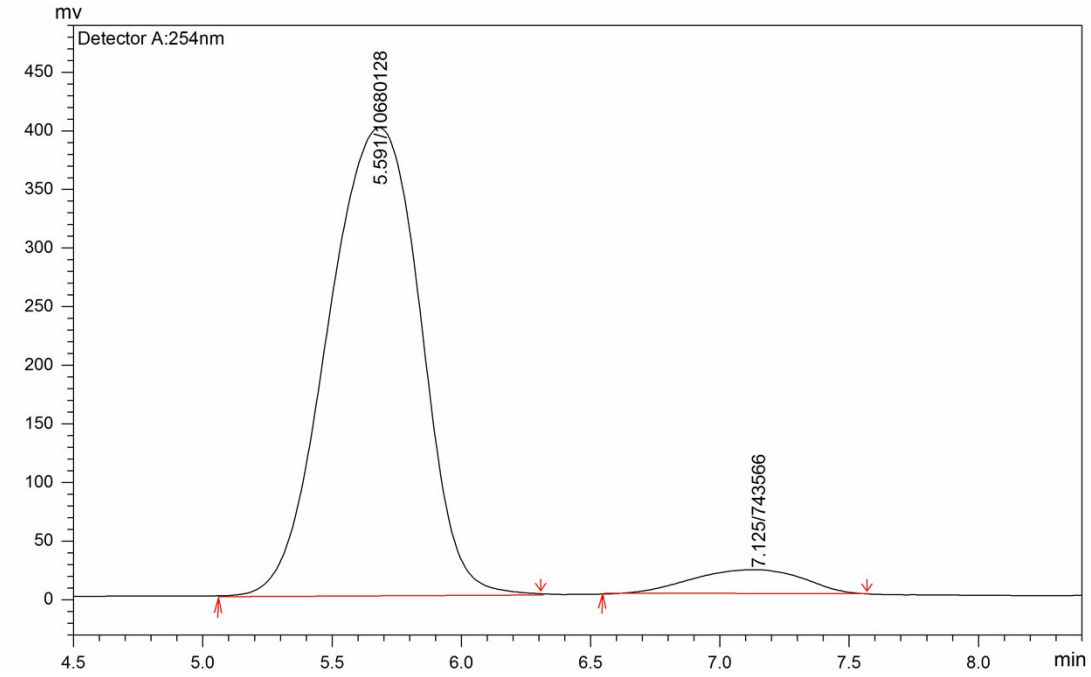

Fig. S20 HLPC of phenyl *n*-butyl sulfoxide obtained over **SiO_2-*IL*-Ti(salen)** (ee value = 87%).

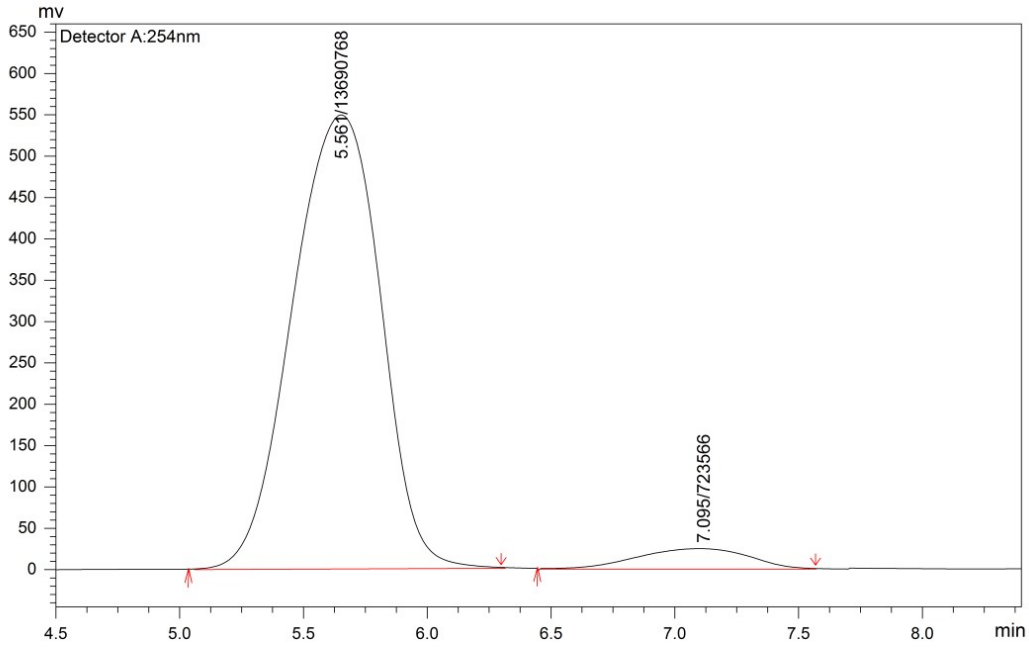

Fig. S21 HLPC of phenyl *n*-butyl sulfoxide obtained over **HO-SiO_2-Ti(salen)$_{0.07}$** (ee value = 90%).

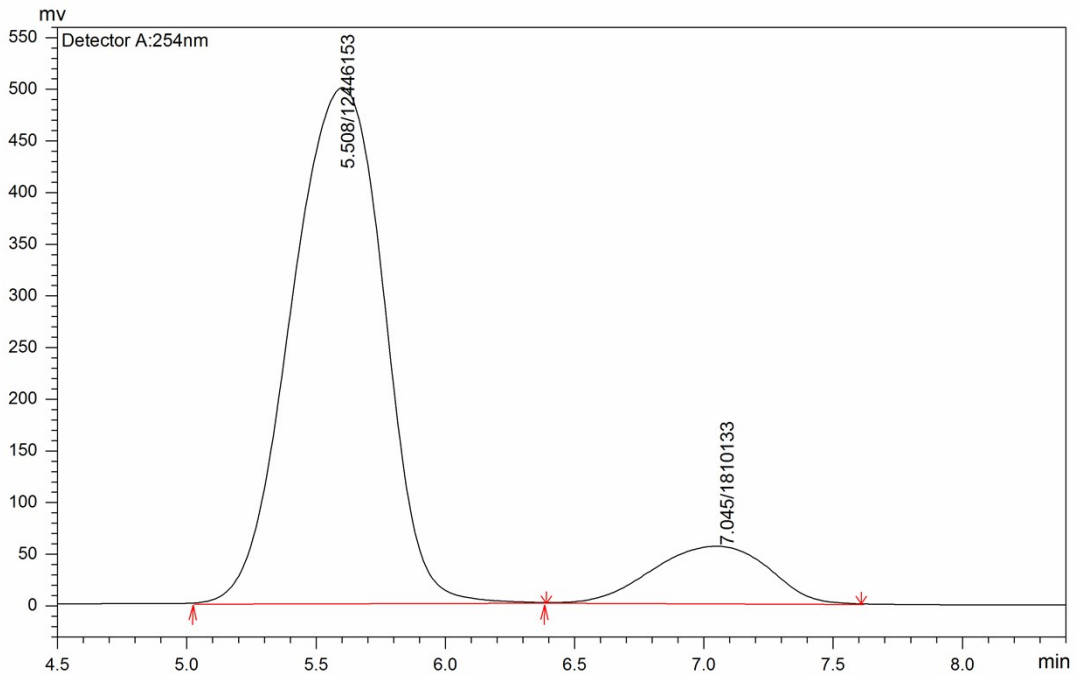

Fig. S22 HLPC of phenyl *n*-butyl sulfoxide obtained over neat complex (ee value = 77%).

Phenyl *n*-hexyl sulfide: The product has been identified by ^{1}H and ^{13}C NMR spectra (see Fig. S23 and S24). ^{1}H NMR ($CDCl_3$, 500 MHz): δ (ppm): 7.32-7.31 (m, 2 H, Ar*H*), 7.28-7.25 (m, 2 H, Ar*H*), 7.16-7.15 (m, 1 H, Ar*H*), 2.76-2.73 (m, 2 H, S-CH_2-), 1.70-1.57 (m, 2 H, S-CH_2-CH_2-), 1.38-1.34 (m, 2 H, S-CH_2-CH_2-CH_2-), 1.24-1.22 (m, 4 H, S-CH_2-CH_2-CH_2-CH_2-CH_2-), 0.83-0.80 (s, 3 H, S-CH_2-CH_2-CH_2-CH_2-CH_2-CH_3). ^{13}C NMR ($CDCl_3$, 125 MHz): δ (ppm): 13.93 (*C*H_3), 22.10 (*C*H_2), 22.34 (*C*H_2), 28.30 (*C*H_2), 31.30 (*C*H_2), 57.32 (*C*H_2), 123.99, 129.17, 130.89, 143.97 (Ar*C*). Chemoselectivity was determined by GC, nitrogen was used as the carrier gas with a flow of 40 mL/min, the injector temperature and the detector temperature were 250 °C, the column temperature was 180 °C, $t_{phenyl\ n\text{-}butyl\ sulfoxide}$ = 3.5 min; ee value was determined by HPLC (*i*-PrOH/ *n*-hexane = 2.5: 7.5 (v/v)); flow rate = 1.0 mL/min; 25 °C; λ = 254 nm; major enantiomer t_R = 5.2 min , minor enantiomer t_S = 6.4 min (see Fig. S25-S28).

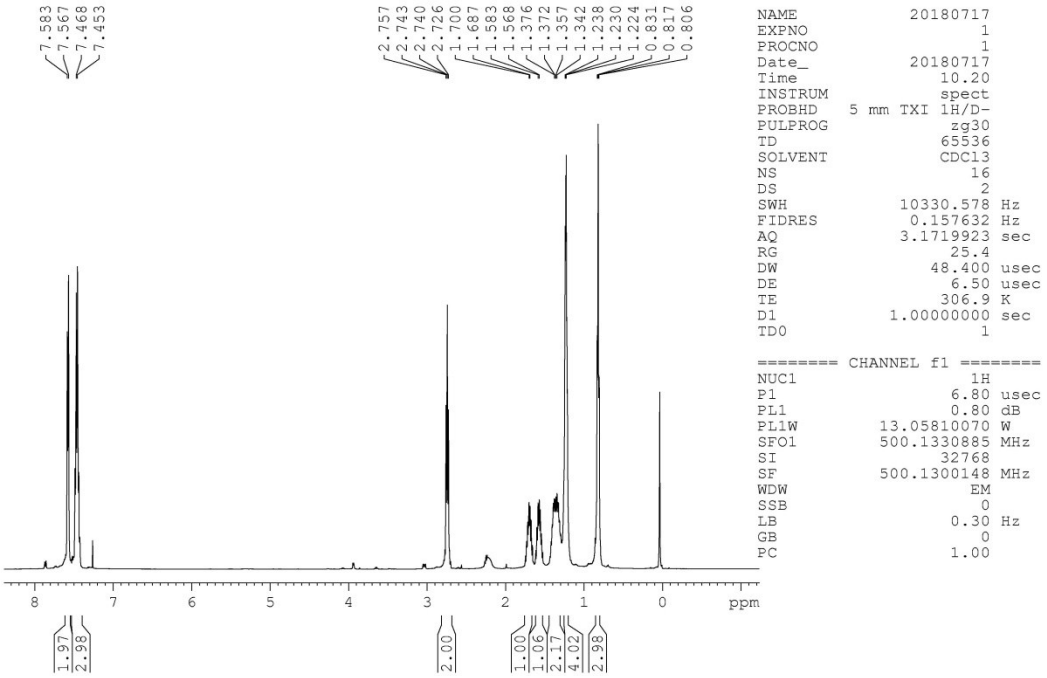

Fig. S23 [1]H NMR of phenyl *n*-hexyl sulfide.

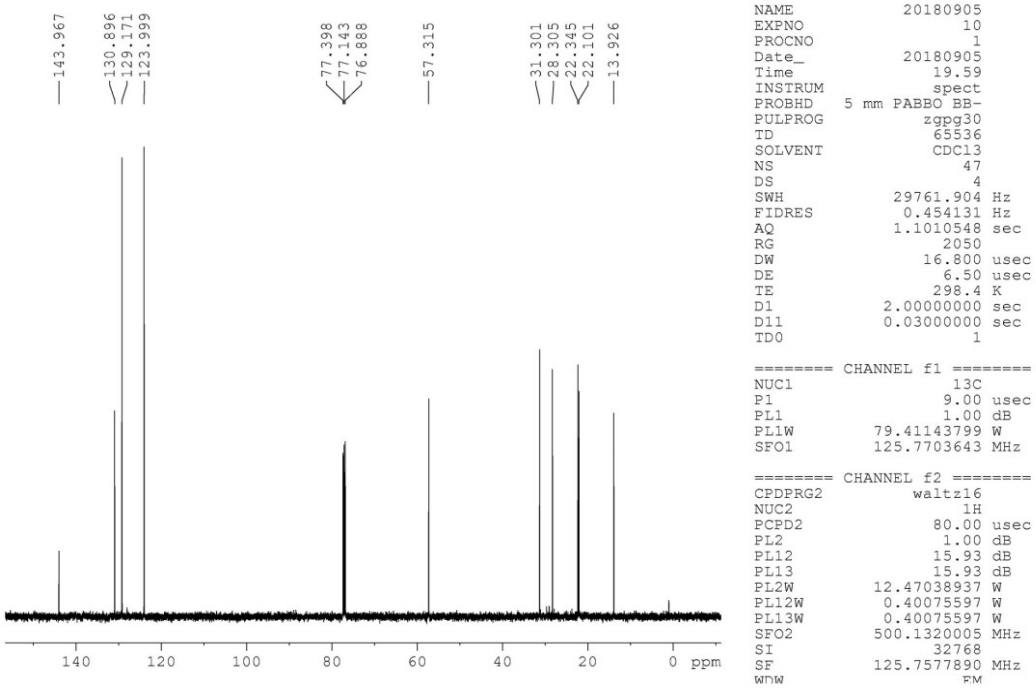

Fig. S24 [13]C NMR of phenyl *n*-hexyl sulfide.

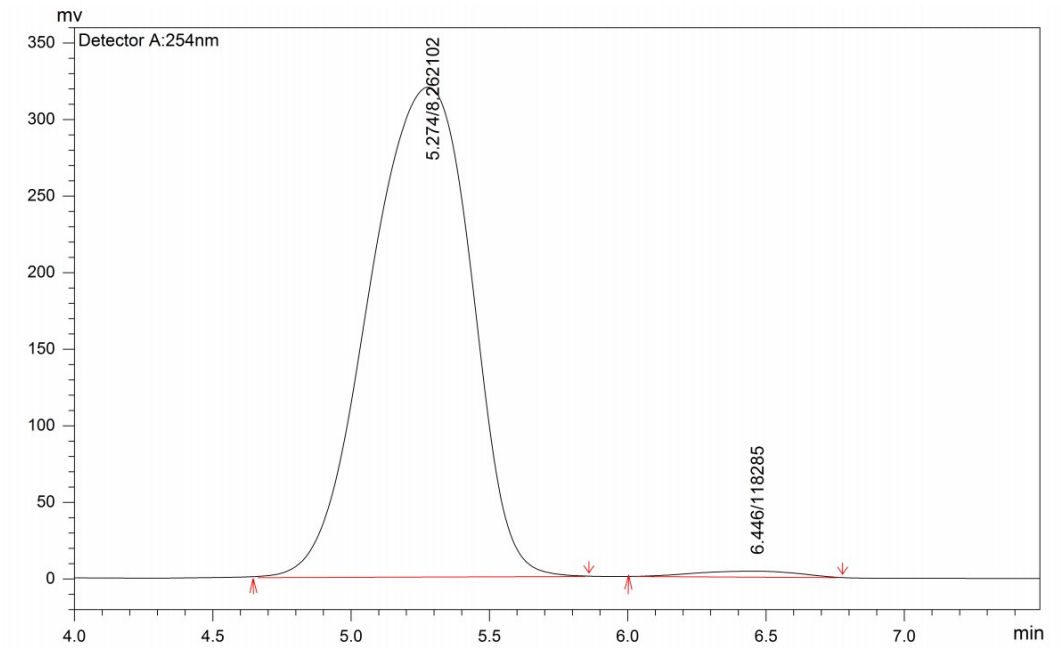

Fig. S25 HLPC of phenyl *n*-hexyl sulfide obtained over **HO-SiO$_2$-*IL*-Ti(salen)$_{0.07}$** (ee value = 97%).

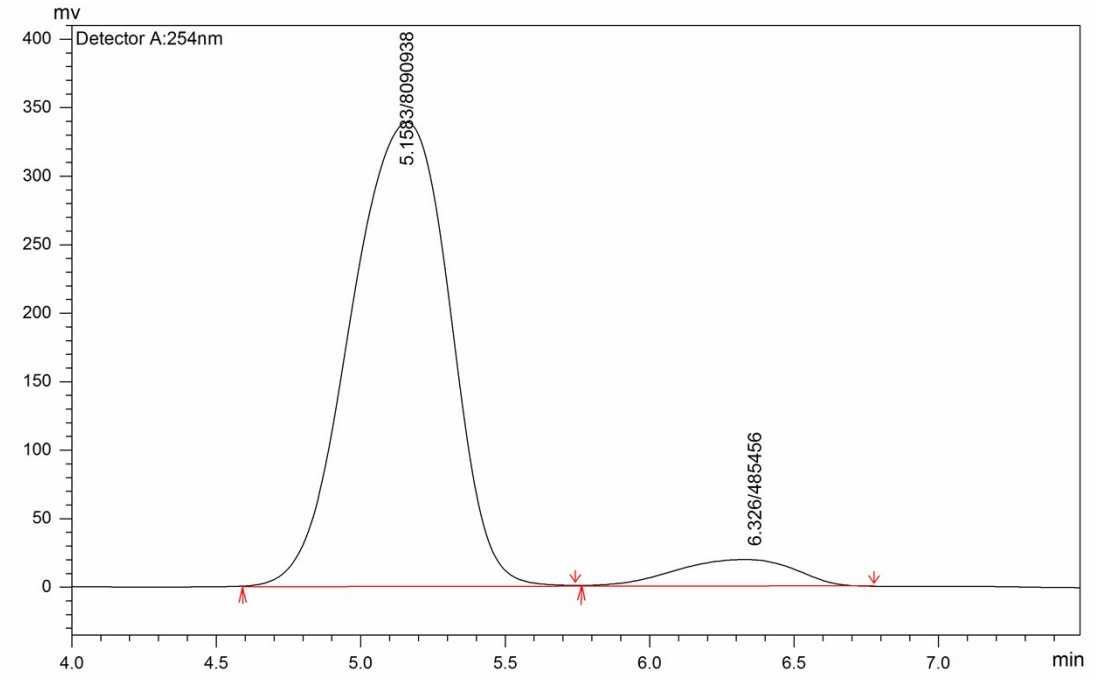

Fig. S26 HLPC of phenyl *n*-hexyl sulfide obtained over **SiO$_2$-*IL*-Ti(salen)** (ee value = 89%).

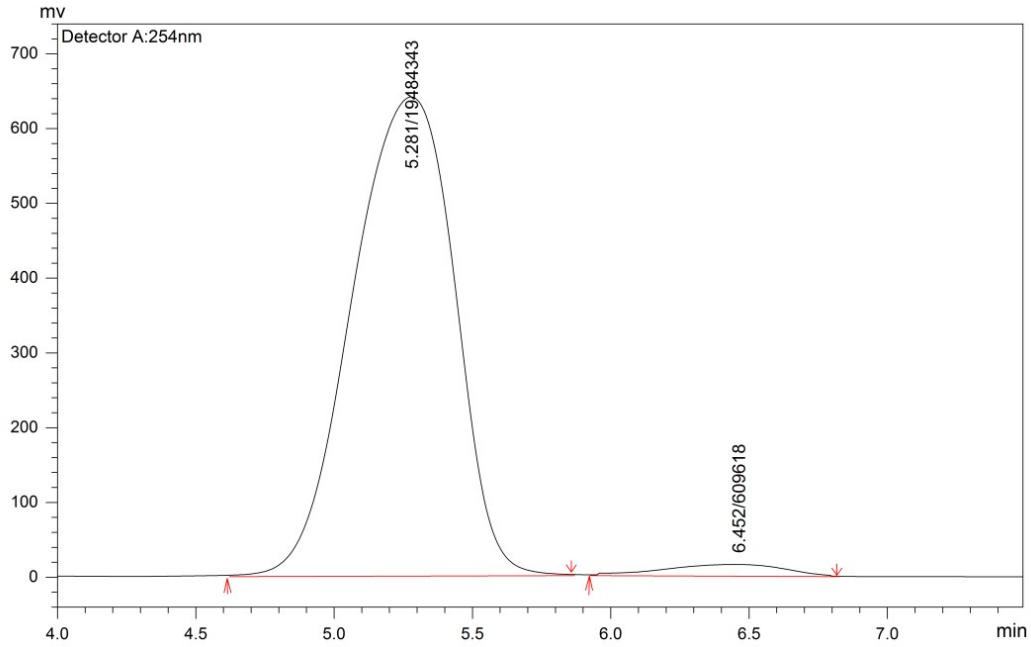

Fig. S27 HLPC of phenyl *n*-hexyl sulfide obtained over **HO-SiO$_2$-Ti(salen)$_{0.07}$** (ee value = 94%).

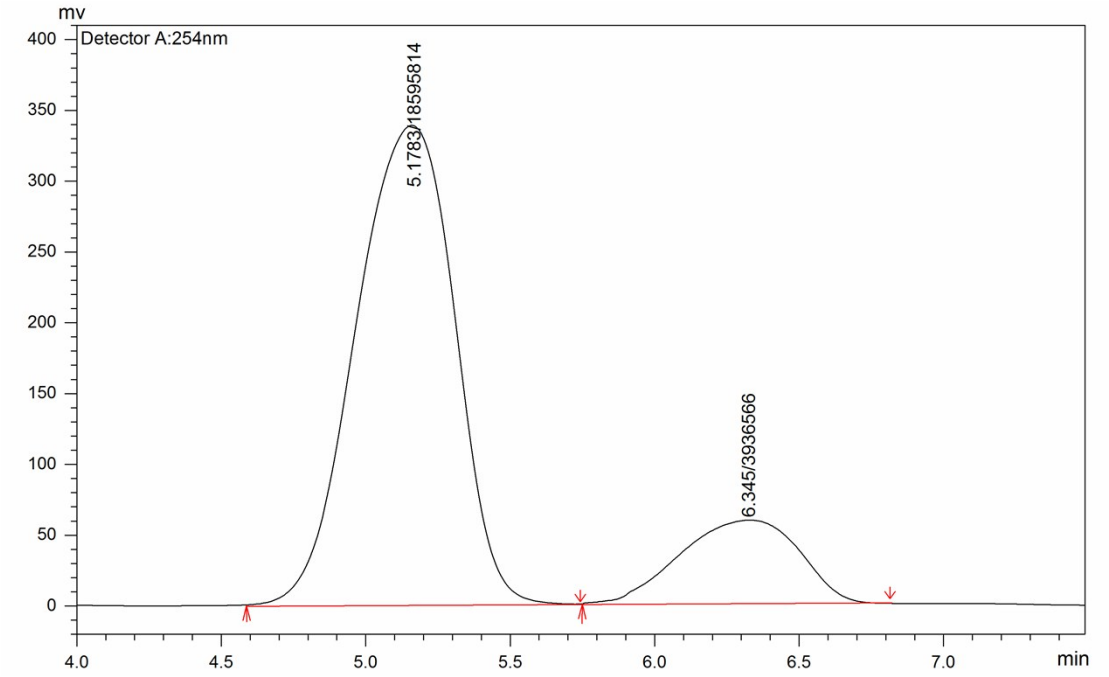

Fig. S28 HLPC of phenyl *n*-hexyl sulfide obtained over neat complex (ee value = 65%).

***p*-Methoxyphenyl methyl sulfoxide**: The product has been identified by ^{1}H and ^{13}C NMR spectra (see Fig. S29 and S30). ^{1}H NMR ($CDCl_3$, 500 MHz): δ (ppm): 7.54-7.52 (d, 2 H, Ar*H*),

6.98-6.96 (d, 2 H, Ar*H*), 3.78 (s, 3 H, -OCH_3), 2.63 (s, 3 H, S-CH_3). ^{13}C NMR ($CDCl_3$, 125 MHz): δ (ppm):43.99 (SCH_3), 55.53 (OCH_3), 114.86, 125.47, 136.59, 161.98 (Ar*C*). Chemoselectivity was determined by GC, nitrogen was used as the carrier gas with a flow of 40 mL/min, injector temperature and detector temperature were 250 °C , column temperature was 180 °C, $t_{p\text{-}methoxyphenyl\ methyl\ sulfoxide}$ = 11.7 min; ee value was determined by HPLC (*i*PrOH/*n*-hexane = 2.5: 7.5 (v/v)); flow rate = 1.0 mL/min; 25 °C; λ = 254 nm; major enantiomer t_R = 9.4 min and minor enantiomer t_S = 11.4 min (see Fig. S31- S34).

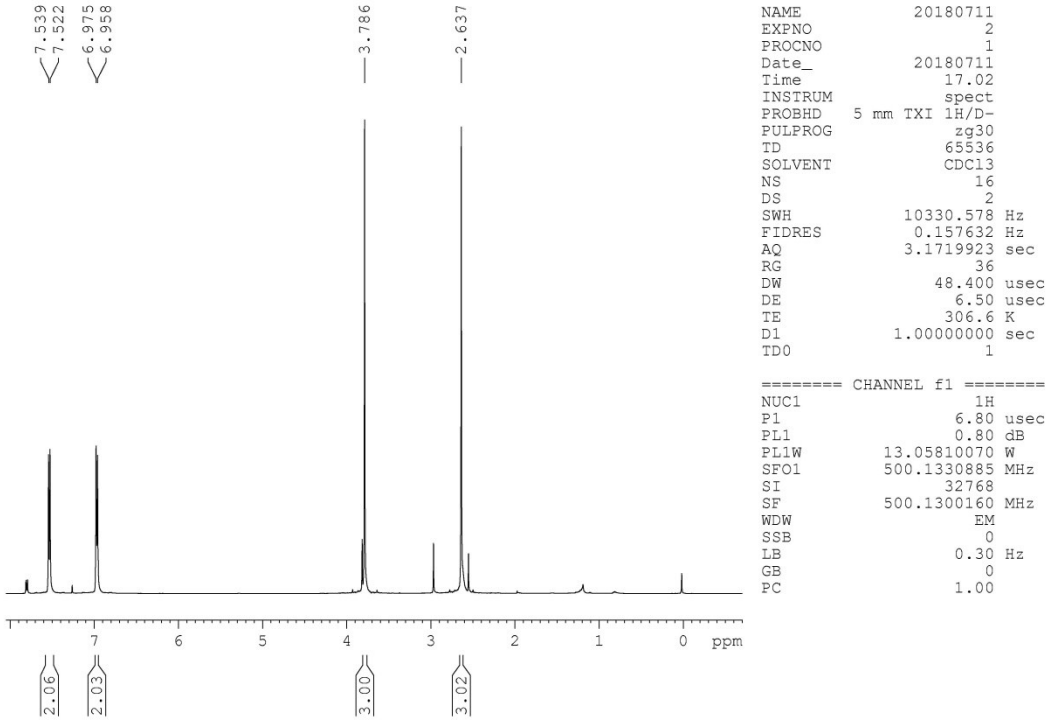

Fig. S29 ^{1}H NMR of *p*-methoxyphenyl methyl sulfoxide.

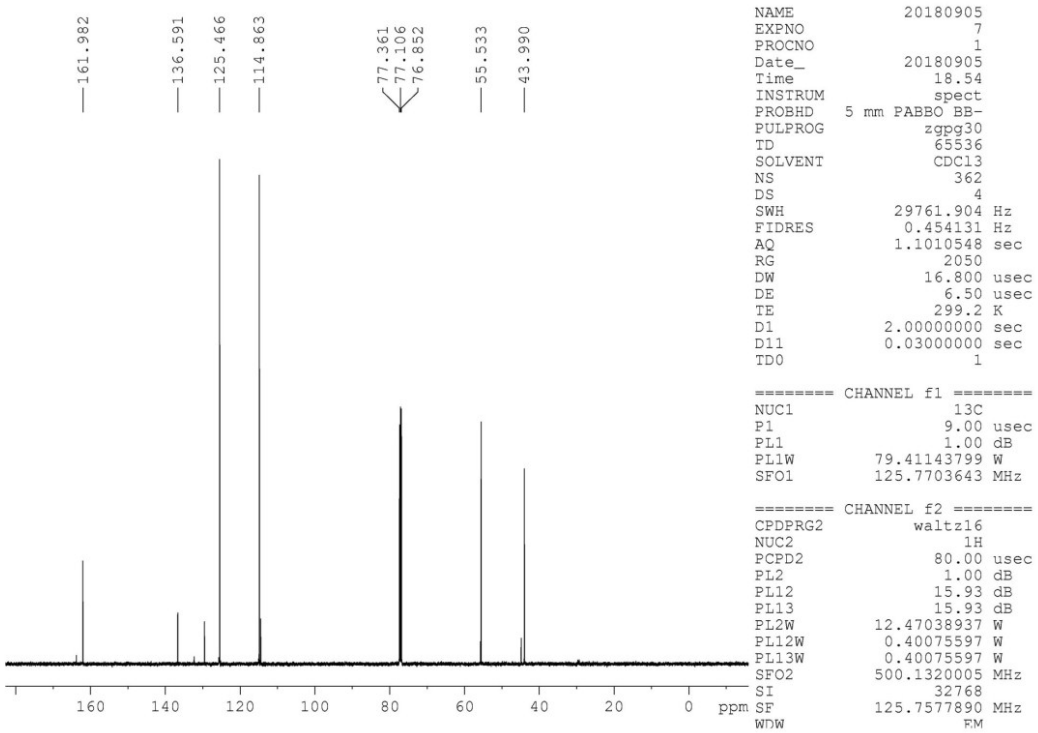

Fig. S30 ^{13}C NMR of *p*-methoxyphenyl methyl sulfoxide.

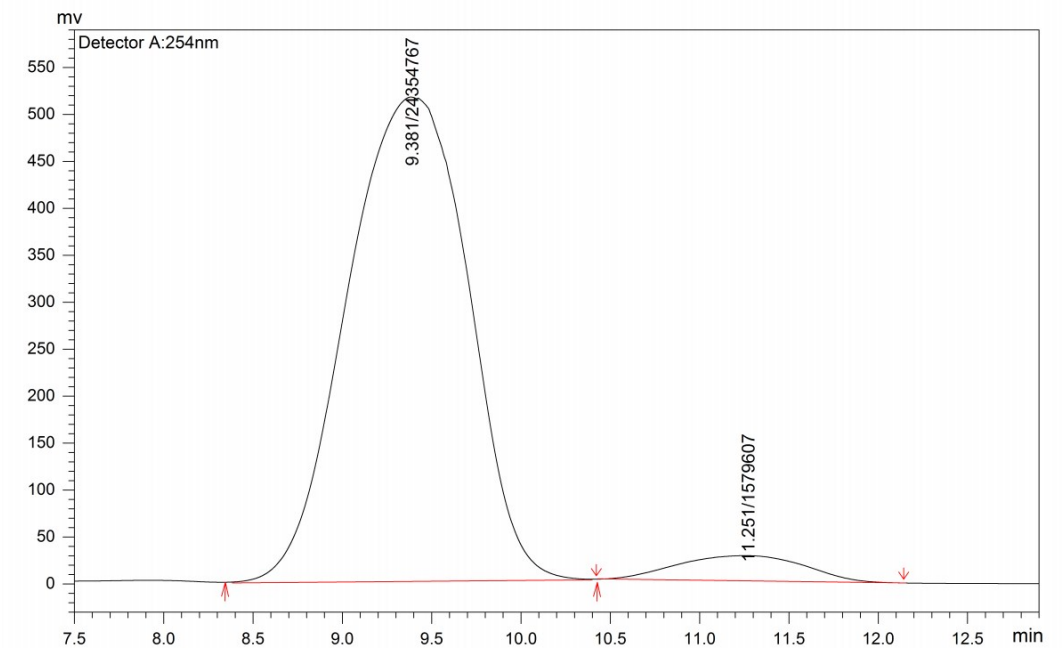

Fig. S31 HLPC of *p*-methoxyphenyl methyl sulfoxide obtained over **HO-SiO$_2$-*IL*-Ti(salen)$_{0.07}$** (ee value = 88%).

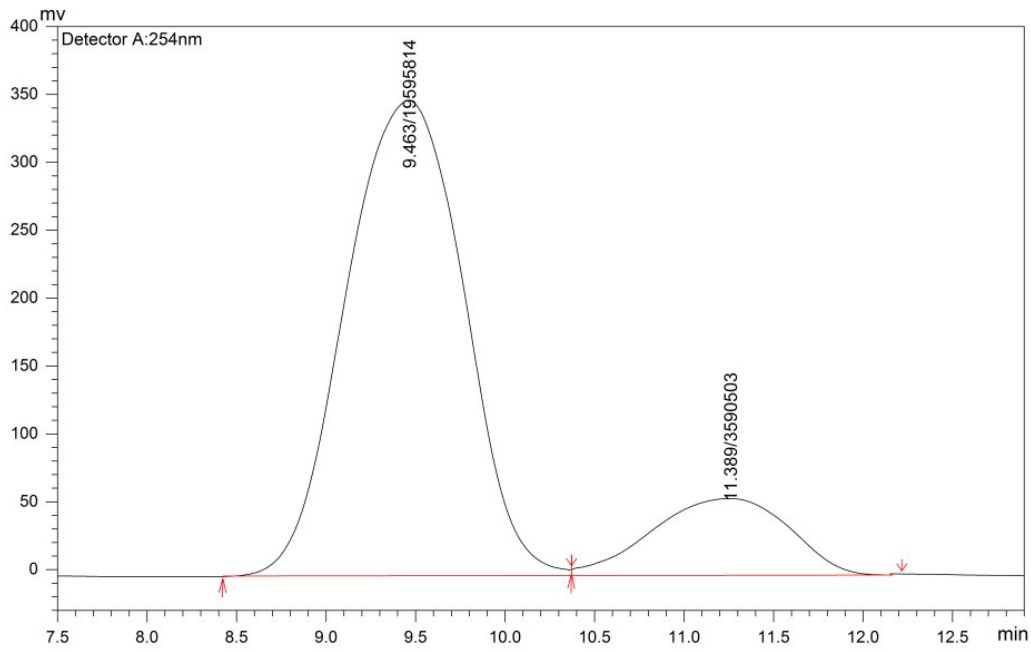

Fig. S32 HLPC of *p*-methoxyphenyl methyl sulfoxide obtained over **SiO_2-*IL*-Ti(salen)** (ee value = 69%).

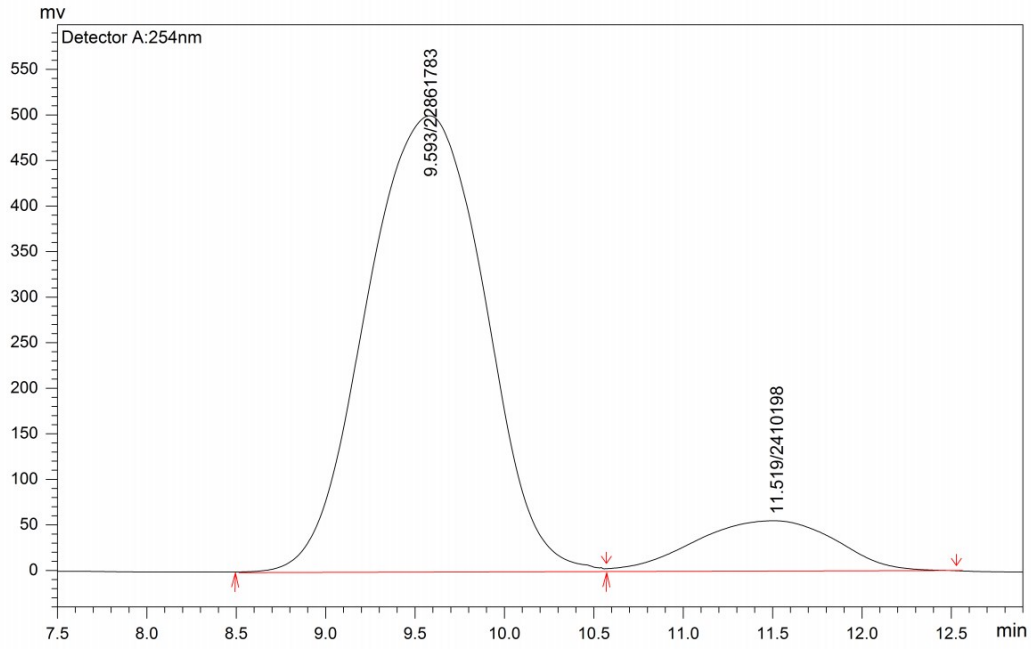

Fig. S33 HLPC of *p*-methoxyphenyl methyl sulfoxide obtained over **HO-SiO_2-Ti(salen)$_{0.07}$** (ee value = 81%).

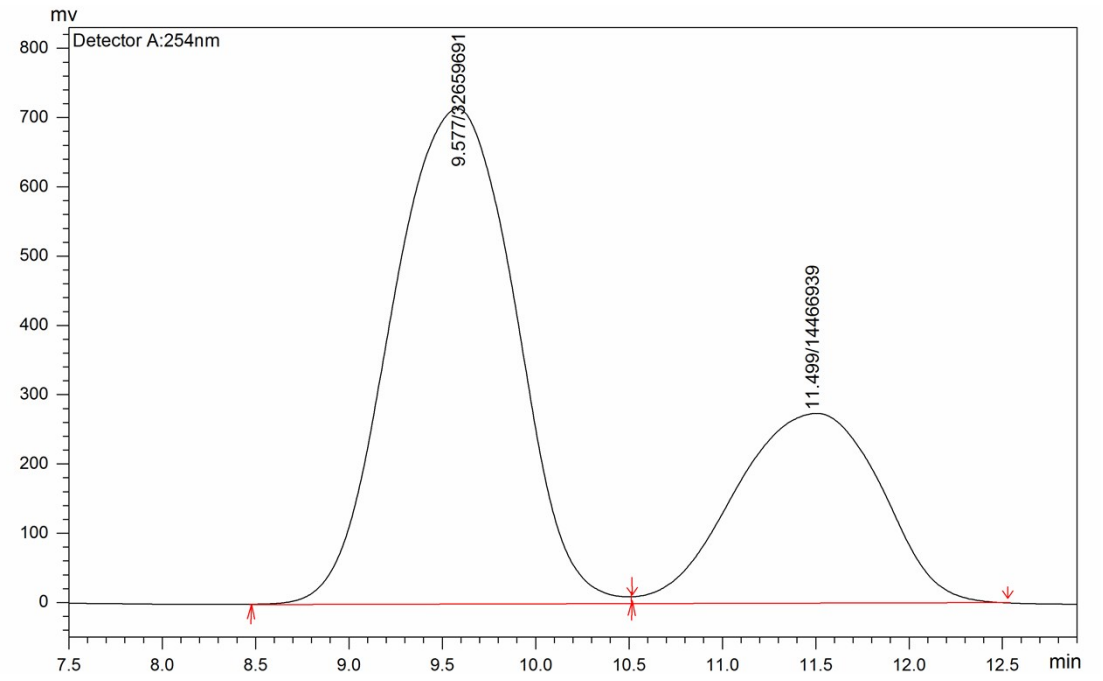

Fig. S34 HLPC of *p*-methoxyphenyl methyl sulfoxide obtained over neat complex (ee value = 49%).

***o*-Methoxyphenyl methyl sulfoxide:** The product has been identified by ^{1}H and ^{13}C NMR spectra (see Fig. S35 and S36). ^{1}H NMR ($CDCl_3$, 500 MHz): δ (ppm): 7.80-7.15 (m, 4 H, Ar*H*), 3.86 (s, 3H, -OCH_3), 2.74 (s, 3 H, S-CH_3). ^{13}C NMR ($CDCl_3$, 125 MHz): δ (ppm): 41.22 (SCH_3), 55.71 (OCH_3), 110.59, 121.71, 124.64, 131.96, 133.12, 154.82 (Ar*C*). Chemoselectivity was determined by GC, nitrogen was used as the carrier gas with a flow of 40 mL/min, injector temperature and detector temperature were 250 °C, the column temperature was 180 °C, $t_{o\text{-}methoxyphenyl\ methyl\ sulfoxide}$ = 9.8 min; ee value was determined by HPLC (*i*-PrOH/*n*-hexane = 2: 8 (v/v)); flow rate = 1.0 mL/min; 25 °C; λ = 254 nm; major enantiomer t_R = 10 min and minor enantiomer t_S =12.2 min (see Fig. S37-S40).

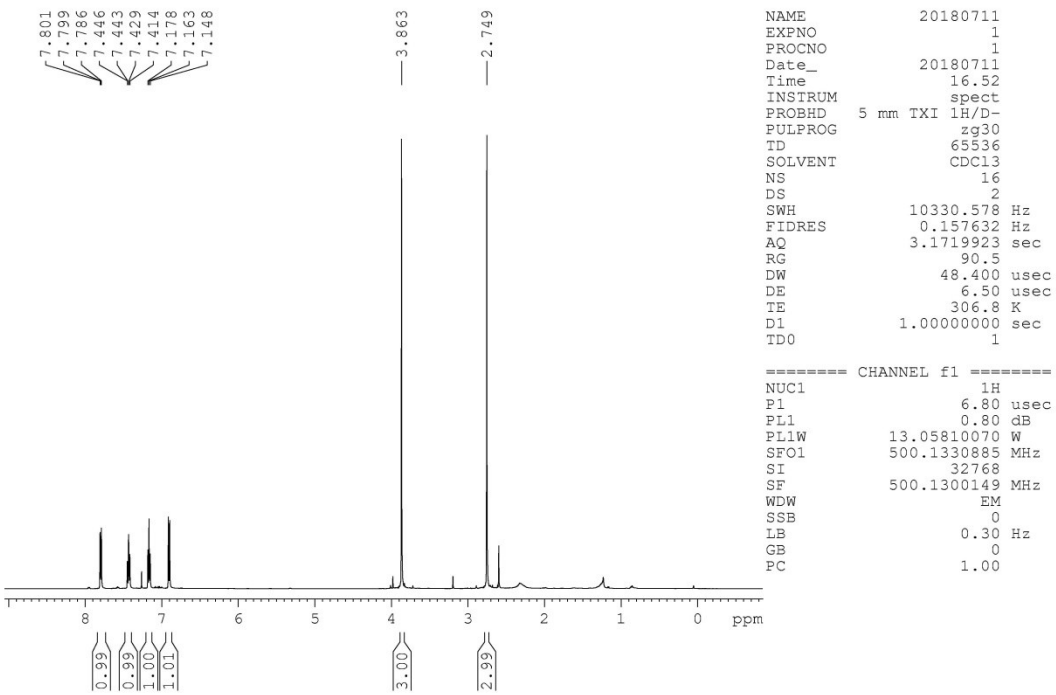

Fig. S35 [1]H NMR of *o*-methoxyphenyl methyl sulfoxide.

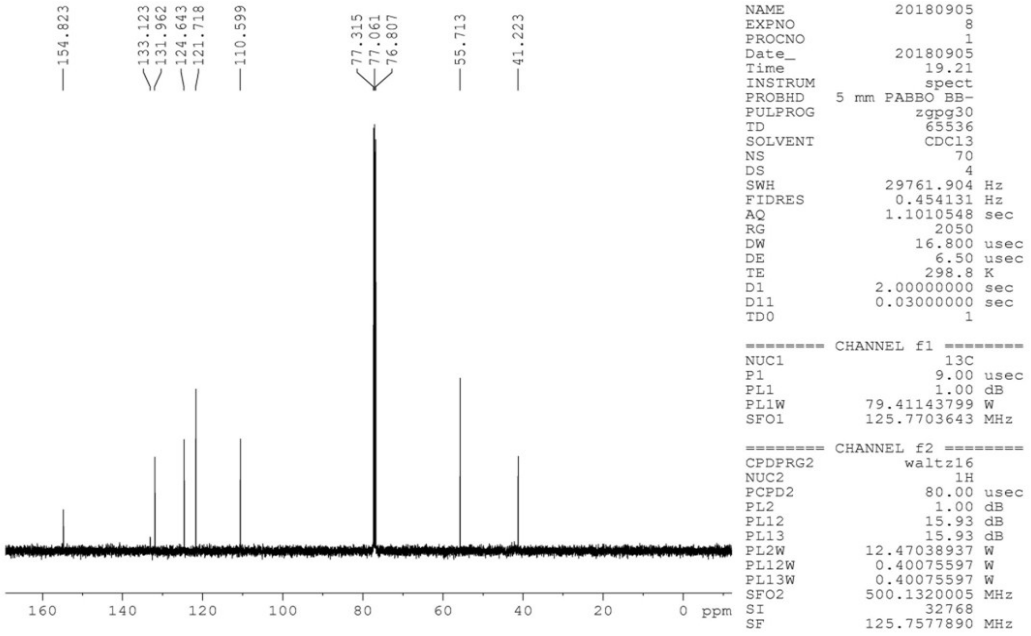

Fig. S36 [13]C NMR of *o*-methoxyphenyl methyl sulfoxide.

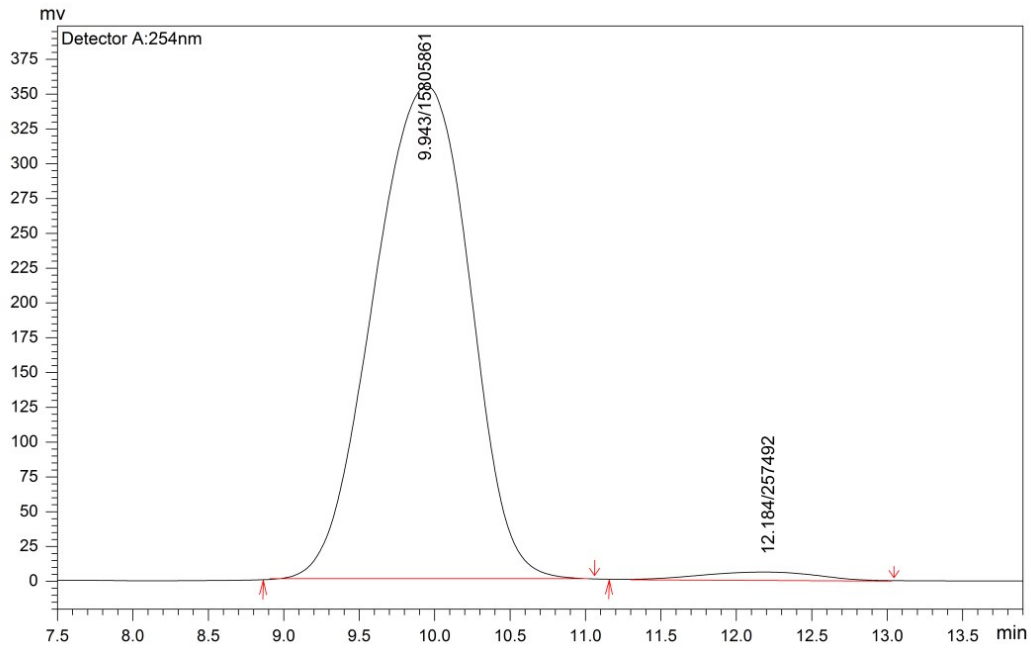

Fig. S37 HLPC of *o*-methoxyphenyl methyl sulfoxide obtained over obtained over **HO-SiO$_2$-*IL*-Ti(salen)$_{0.07}$** (ee value = 97%).

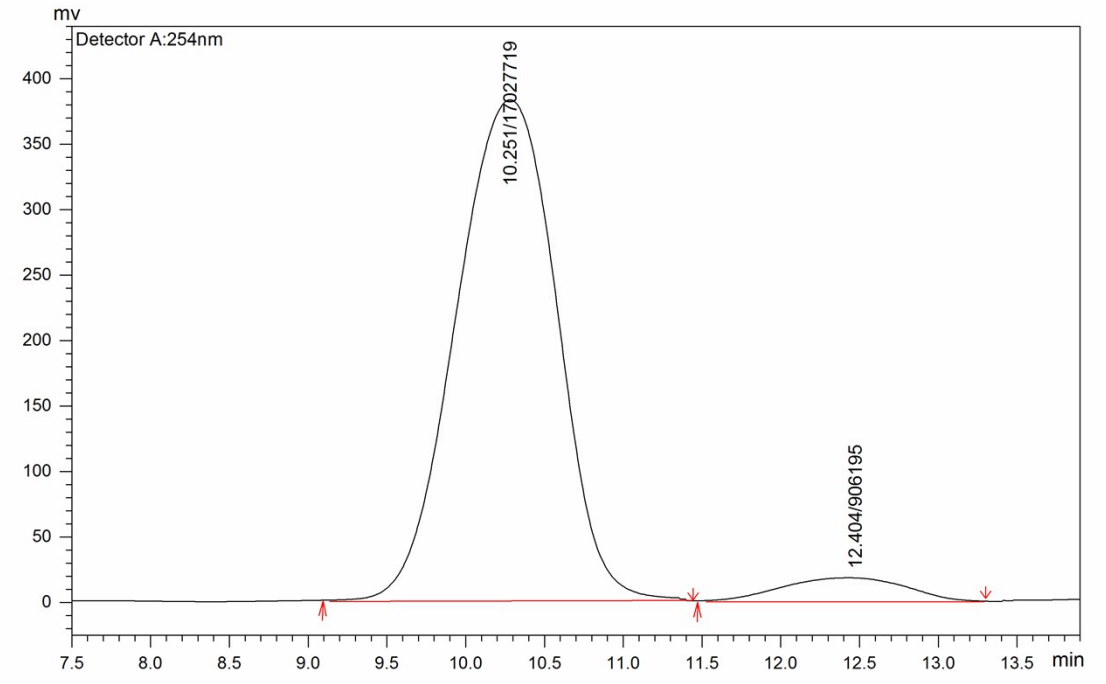

Fig. S38 HLPC of *o*-methoxyphenyl methyl sulfoxide obtained over **SiO$_2$-*IL*-Ti(salen)** (ee value = 90%).

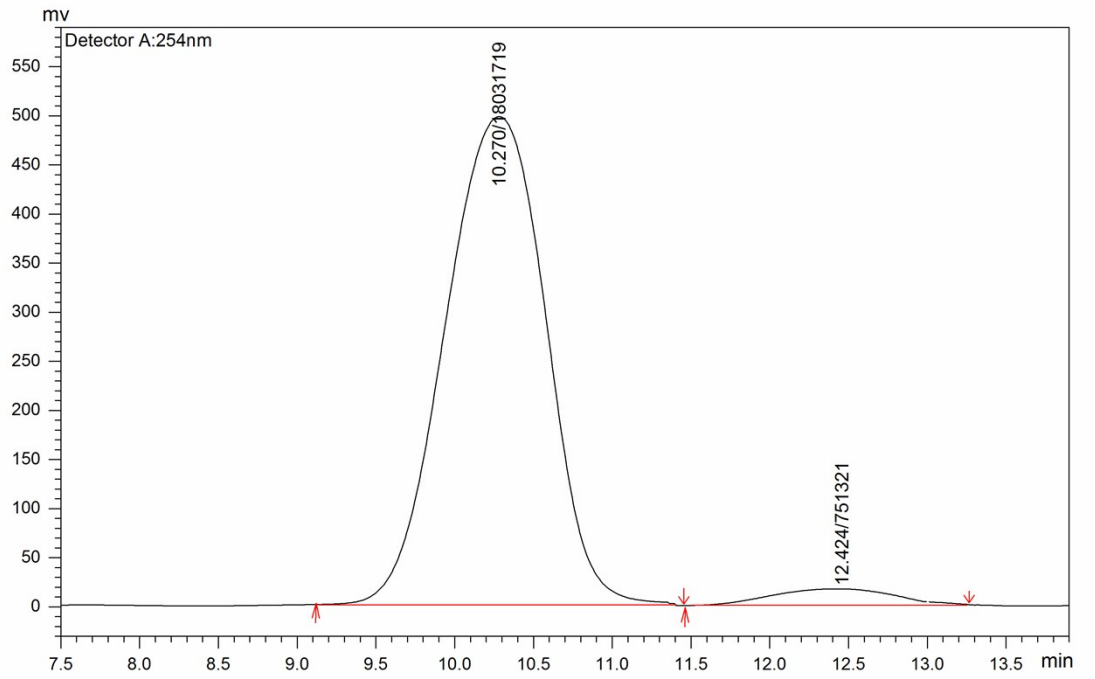

Fig. S39 HLPC of *o*-methoxyphenyl methyl sulfoxide obtained over **HO-SiO$_2$-Ti(salen)$_{0.07}$** (ee value = 92%).

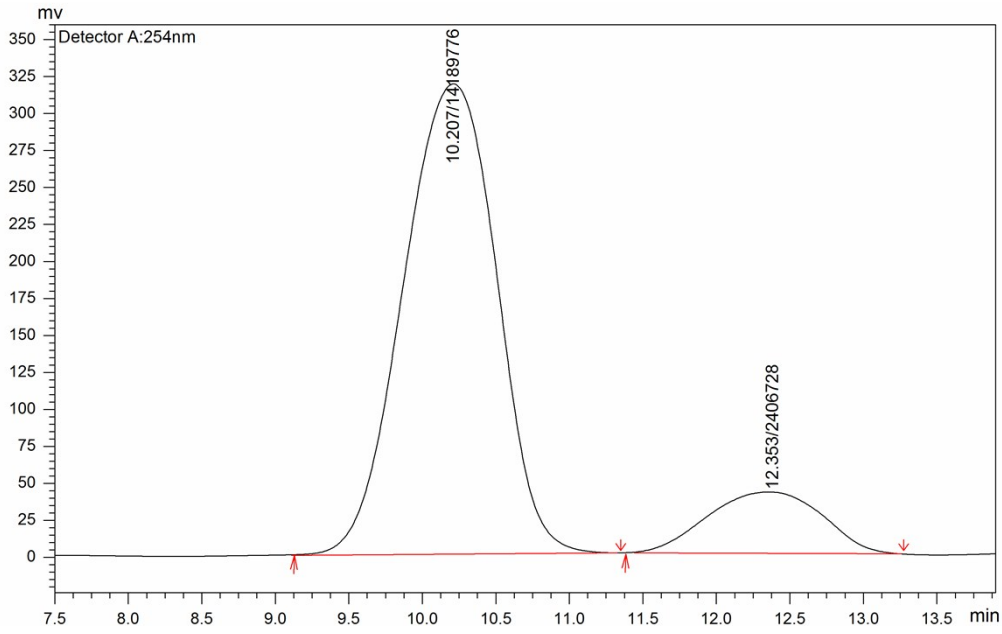

Fig. S40 HLPC of *o*-methoxyphenyl methyl sulfoxide obtained over neat complex (ee value = 71%).

***p*-Bromophenyl methyl sulfoxide**: The product has been identified by ^{1}H and ^{13}C NMR spectra (see Fig. S41 and S42). ^{1}H NMR ($CDCl_3$, 500 MHz): δ (ppm): 7.66-7.65 (d, 2 H, Ar*H*), 7.52-7.50 (d, 2 H, Ar*H*), 2.70 (s, 3 H, S-CH_3). ^{13}C NMR ($CDCl_3$, 125 MHz): δ (ppm): 43.96 (S*C*H_3), 125.17, 125.49, 132.59, 144.82 (Ar*C*). Chemoselectivity was determined by GC, nitrogen was used as the carrier gas with a flow of 40 mL/min, injector temperature and detector temperature were 250 °C, the column temperature was 180 °C, $t_{p\text{-}bromophenyl\ methyl\ sulfoxide}$ = 11.2 min; ee value was determined by HPLC (*i*-PrOH/*n*-hexane = 2.5: 7.5 (v/v)); flow rate = 1.0 mL min^{-1}; 25 °C; λ = 254 nm; major enantiomer t_R = 8.0 min and minor enantiomer t_S =9.8 min (see Fig. S43-S46)

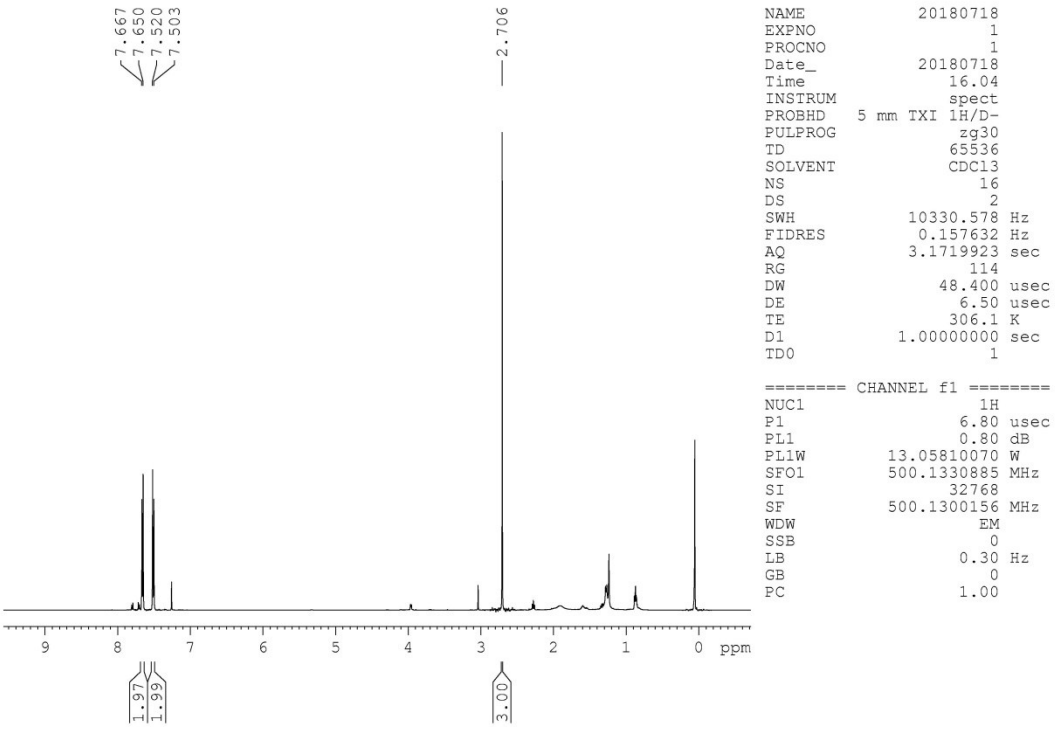

Fig. S41 ^{1}H NMR of *p*-bromophenyl methyl sulfoxide.

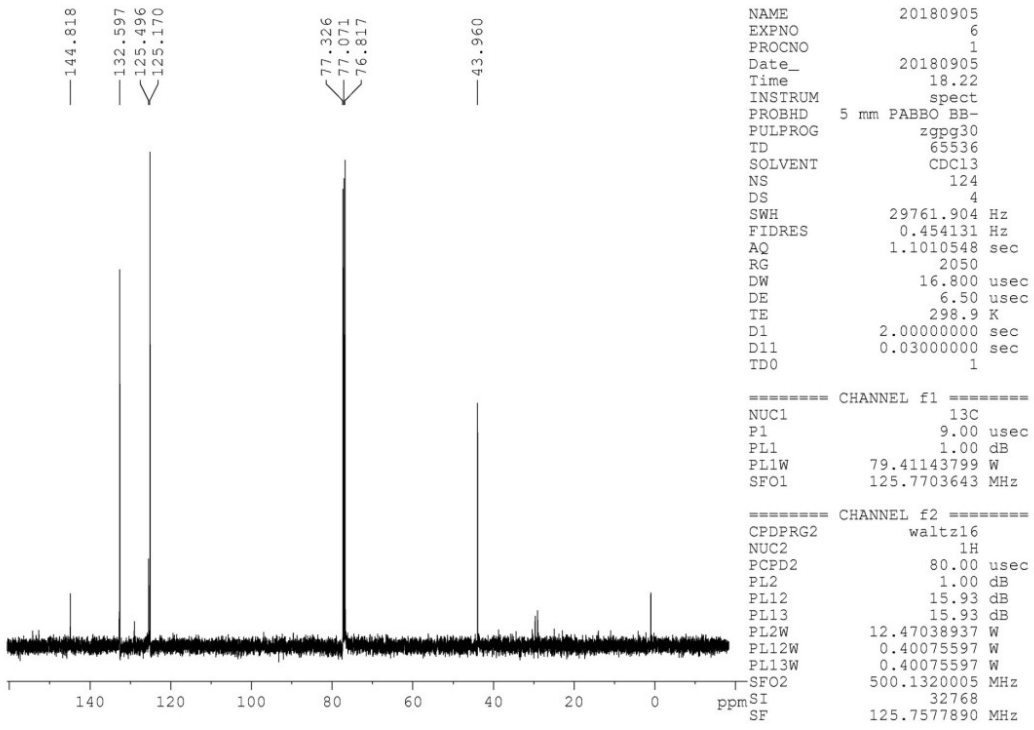

Fig. S42 ^{13}C NMR of *p*-bromophenyl methyl sulfoxide.

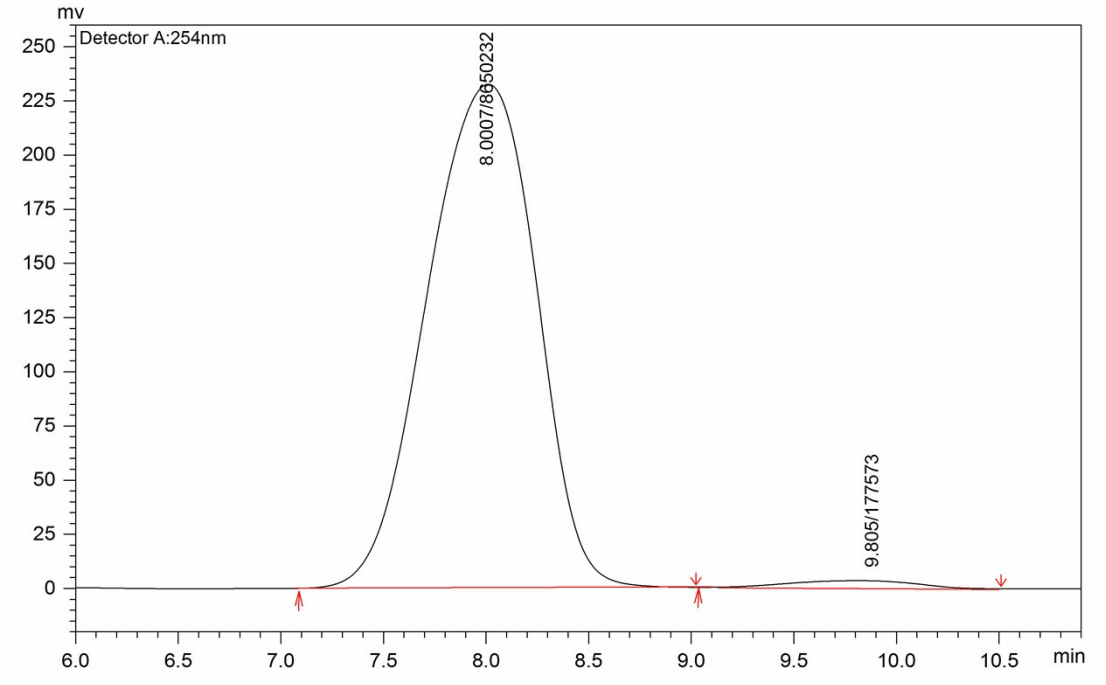

Fig. S43 HLPC of *p*-bromophenyl methyl sulfoxide obtained over **HO-SiO$_2$-*IL*-Ti(salen)$_{0.07}$** (ee value = 95%).

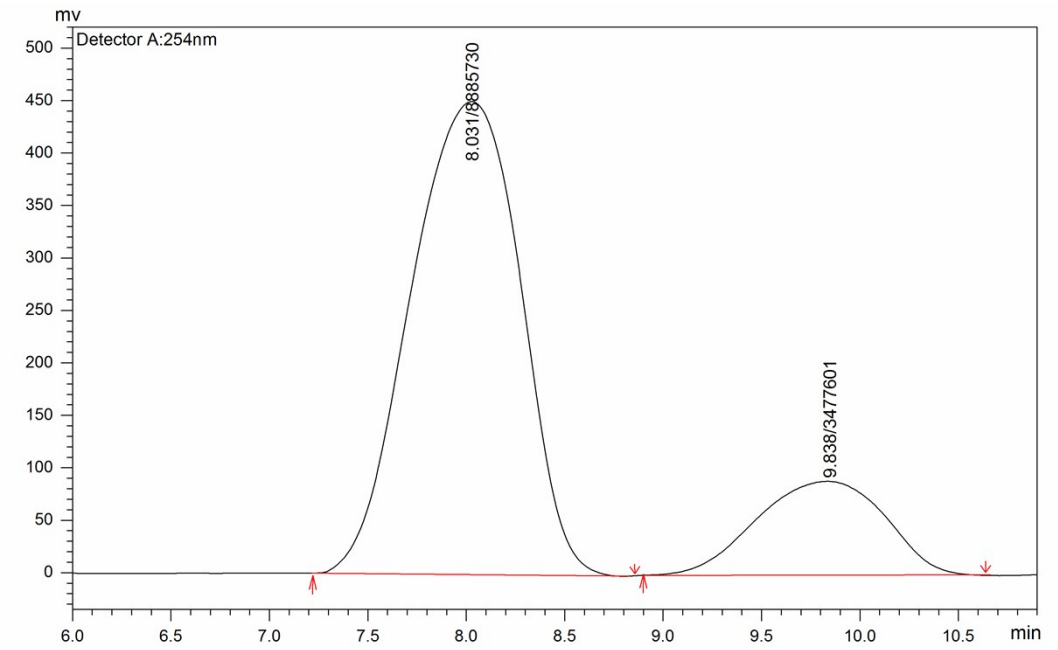

Fig. S44 HLPC of *p*-bromophenyl methyl sulfoxide obtained over **SiO_2-*IL*-Ti(salen)** (ee value = 68%).

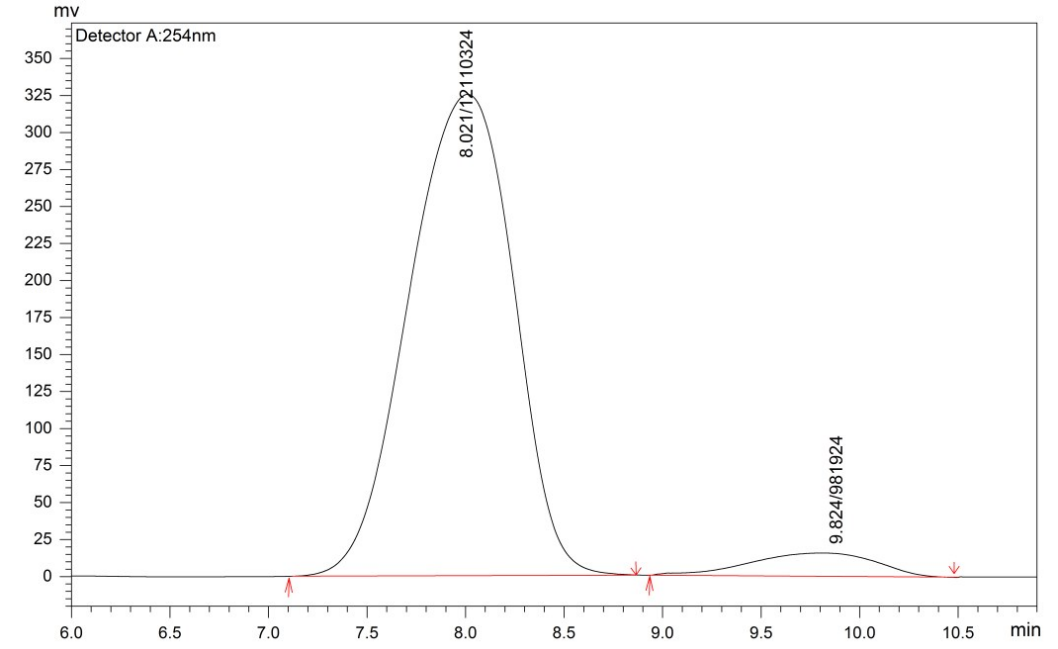

Fig. S45 HLPC of methyl *p*-bromophenyl sulfoxide obtained over **HO-SiO_2-Ti(salen)$_{0.07}$** (ee value = 85%).

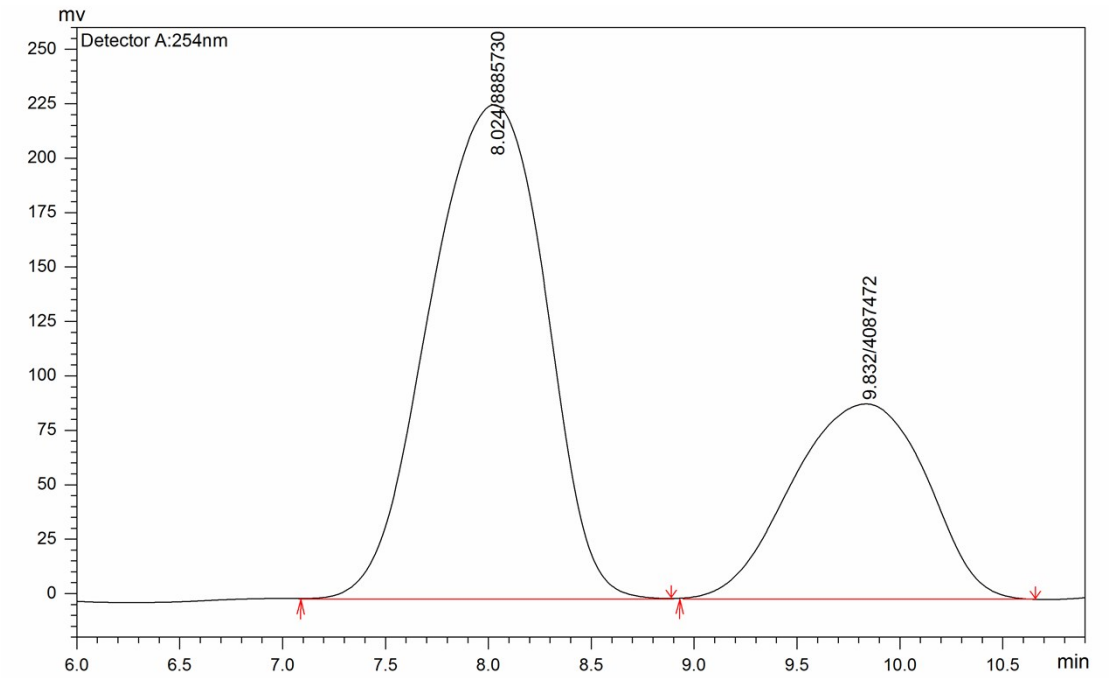

Fig. S46 HLPC of *p*-bromophenyl methyl sulfoxide obtained over neat complex (ee value = 38%).

3.2 Asymmetric sulfoxidation for kinetic measurement

Kinetics was employed to further evaluate the advantage of Pickering interfacial catalysis as well as the positive effects of IL moiety on the catalytic efficiency. The selected catalyst (1.25 mol% of substrate) was stirred with methyl pheny sulfide (0.5 mmol) in deionized water (1.0 mL) at 25 °C. H_2O_2 (30 *wt.*%, 0.6 mmol) was then added into the mixture within 5 min. To determine the rate of sulfoxidation, aliquots at an interval of 15 min were drawn from the reaction mixture, filtered through organic membrane with ethyl acetate as an extracting agent, and analyzed by GC.

Corresponding kinetic curves and rate curves are shown in Fig. S47. Clearly, **HO-SiO_2-*IL*-Ti(salen)$_{0.07}$** benefitted from the amphiphilic Janus characteristic, affording higher efficiency than the uniform particle of **SiO_2-*IL*-Ti(salen)** (Fig. S47a *vs.* S47c). This observation demonstrated that Pickering interfacial catalysis indeed promoted aqueous sulfoxidation through the formation of stable Pickering emulsion. Actually, apart from maximizing the interfacial contact area to

promote mass transfer, the emulsion droplet created a confined hydrophobic environment for the aqueous catalysis. It was evident from the gradient increase in the conversion of sulfide over **HO-SiO$_2$-*IL*-Ti(salen)$_{0.07}$** (Fig. S47A-a). The corresponding observed rate constant (k_{obs}) initially rose rapidly due to the dramatically increasing concentration of reactants in hydrophobic compartments during emulsification, went through a maximum, and then drastically decreased due to a dilution effect (Fig. S47B-a). The confined catalysis together with interfacial catalytic effects synergistically resulted in high efficiency of **HO-SiO$_2$-*IL*-Ti(salen)$_{0.07}$** in the aqueous asymmetric sulfoxidation. While, despite also Pickering interfacial catalysis, the k_{obs} over **HO-SiO$_2$-Ti(salen)$_{0.07}$** was always lower than that over **HO-SiO$_2$-Ti(salen)$_{0.07}$** (Fig. S47b *vs.* S47a). The observations agreed with active role of the imidazolium-based IL linker in the overall reaction mechanism, which ensured conformational freedom of the active sites, enhanced mass transfer of regents and stabilized the reactive intermediates. The high efficiency of **HO-SiO$_2$-*IL*-Ti(salen)$_{0.07}$** was consistent with our hypothesis that enhanced interphase mass transfer, as well as synergistic action of dense active species, was crucial for efficient aqueous sulfoxidation, and this could be achieved by endowing chiral salen Ti^{IV} catalyst with interfacial activity. For this reason, it was not surprising that the traditional neat complex was inactive and provided the lowest k_{obs} in water due to the poor water-solubility of catalyst and sulfide (Fig. S47d).

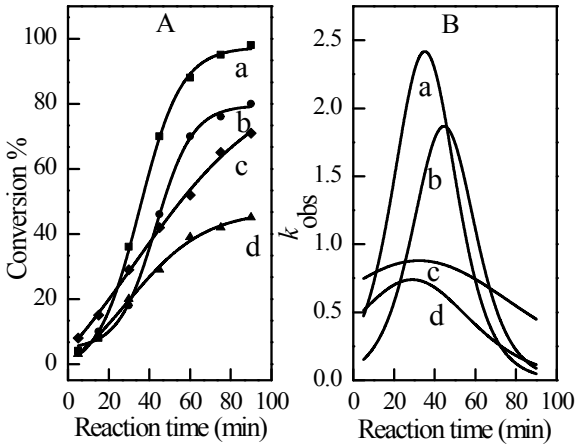

Fig. S47 Fitted kinetic curves (A) and rate curves (B) of asymmetric sulfoxidation of methyl phenyl sulfide by **HO-SiO$_2$-*IL*-Ti(salen)$_{0.07}$** (a), **HO-SiO$_2$-Ti(salen)$_{0.07}$** (b), **SiO$_2$-*IL*-Ti(salen)** (c), and neat complex (d) in water.

References

(1) W. Stober, A. Fink, E. Bohn, E. Controlled. Growth of Monodisperse Silica Spheres in the Micron Size Range. *J. Colloid Interface Sci.,* **1968**, *26*, 62-69.

(2) S. colonna, R. fornasier. *N*-Dodecyl-*N*-methylphedrinium bromide: a specific catalyst for the borohydride reduction of carbonyl compounds under phase-transfer conditions. *Synthesis*, **1975**, *8*, 531-532.

(3) C. Lv, D. Xu, S. Wang, W. Sun. A practical Ti-salen catalyst based on dimeric salen ligand for asymmetric addition of trimethylsilyl cyanide to aldehydes. *Catal. Commun.,* **2011**, *12*, 1242-1245.

(4) J. Kim, G. Kim. Enantioselectivities of chiral Ti(IV) salen complexes immobilized on MCM-41 in asymmetric trimethylsilylcyanation of benzaldehyde. *Catal. Lett.,* **2004**, *92*, 123-130.

(5) A. Perro, F. Meunier. Production of large quantities of “Janus” nanoparticles using wax-in-

water emulsions. *Colloids Surf., A*, **2009**, *332*, 57–62.

(6) S. Jiang, Q. Chen, M. Tripathy, S. Granick. Janus particle synthesis and assembly. *Adv. Mater.*, **2010**, *22*, 1060–1071.

(7) G. Y. Fang, Z. Chen, H. Li. Synthesis and properties of microencapsulated paraffin composites with SiO_2 shell as thermal energy storage materials. *Chem. Eng. J.*, **2012**, *163*, 154.

(8) F. Song, C. Wang, J. M. Falkowski, L. Ma, W. Lin. Isoreticular chiral metal−organic frameworks for asymmetric alkene epoxidation: Tuning catalytic activity by controlling framework catenation and varying open channel sizes. *J. Am. Chem. Soc.,* **2010**, *132*, 15390.

(9) C. E. Song, E. J. Roh, Practical method to recycle a chiral (salen)Mn epoxidation catalyst by using an ionic liquid. *Chem. Commun.,* **2000**, *10*, 837

(10) S. Arditty, V. Schmitt, F. Lequeux, F. Leal-Calderon. Interfacial properties in solid-stabilized emulsions, *Eur. Phys. J. B,* **2005**, *44*, 381–393.

(11) F. Tu, B. J. Park, D. Lee. Thermodynamically stable emulsions using Janus dumbbells as colloid surfactants. *Langmuir*, **2013**, *29*, 12679-12687.